

## **ESIPT-based probes for cations, anions and neutral species: Recent progress, multidisciplinary applications and future perspectives**

**Nidhi Nehra<sup>a,b</sup>, Rahul Kaushik<sup>c,d\*</sup>**

<sup>a</sup>School of Chemical Sciences, Indian Association for the Cultivation of Sciences, Kolkata -700032, INDIA

<sup>b</sup>Department of Chemistry, Indian Institute of Technology, Powai, Mumbai- 400 076, India

<sup>c</sup>Chemical Oceanography Division, CSIR- National Institute of Oceanography, Dona Paula- 403004, Goa, India

<sup>d</sup>Academy of Scientific and Innovative Research (AcSIR), Ghaziabad- 201002, India.

ORCID ID: 0000-0002-1854-1118, Email: krahul@nio.org and rkphdresearchwork@gmail.com

### **Abstract**

Fluorescent and colourimetric probes for small analytes (cations, anions and neutral molecules) have drawn significant attention in recent years. These probes interact with analytes and induce spectral change due to the variations in the photo-physical properties of the fluorophore/chromophore used. Among several photo-physical mechanisms, ESIPT (Excited State Intramolecular Proton Transfer) based probes are more advantageous due to their photo-physical properties viz. solvent polarity effect, large spectral shift with multi-channel fluorescence, high quantum yield etc. In recent years, ESIPT-based probes have shown several promising applications, especially monitoring small analytes in biological samples, smartphone app-assisted heavy metal detection in environmental samples, inkless writing, anti-counterfeiting applications etc. Therefore, this review is dedicated to recently reported ESIPT-based probes for small analytes. We have highlighted the organic units responsible for the ESIPT mechanism, their photo-physical parameters, selectivity and sensitivity properties and recent advances in their applications.

**Keywords:** Chemical sensors, ESIPT, keto-enol tautomerism, Fluorescent probes, colorimetric probes, small-analyte sensors

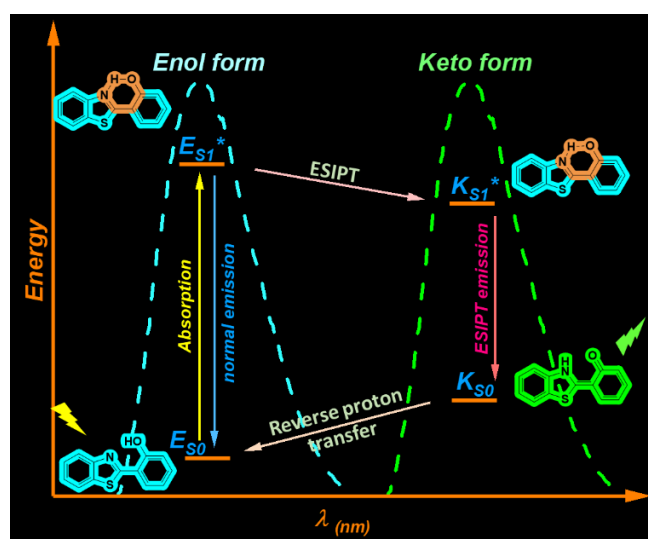
## Introduction

Optical sensors have drawn remarkable attention in recent years owing to their multidisciplinary applications.<sup>1, 2</sup> Optical sensors (colourimetric and/or fluorescent sensors) display high sensitivity and can induce absorbance or fluorescence spectral change when interacting with analytes concentration at  $\mu\text{M}$ - $\text{nM}$  levels.<sup>3-5</sup> These probes have several advantages including cost-effectiveness, easy synthesis, quick response time, application in biological samples without sample destruction and many more.<sup>6, 7</sup> For the detection of small analytes, traditional methods have been used which are tedious, destructive and require expert personnel for instrument handling and sample preparation. In contrast, UV-vis and fluorescent probes do not require such expert manpower due to their easy instrument operations. Therefore, several colourimetric and fluorescent probes have been designed for sensing small analytes such as toxic anions (sulfide<sup>8, 9</sup>, cyanide<sup>10</sup>, fluoride<sup>11</sup>, acetate<sup>11</sup> etc.), toxic cations<sup>12, 13</sup> ( $\text{Hg}^{2+}$ ,  $\text{Cu}^{2+}$ ,  $\text{Zn}^{2+}$ ,  $\text{Pb}^{2+}$  etc.) and neutral species ( $\text{H}_2\text{O}_2$ <sup>14</sup>,  $\text{HCHO}$ <sup>15</sup>, moisture<sup>16, 17</sup>, bio-thiols<sup>18, 19</sup> etc.).

Small analytes (cations, anions and neutral molecules) are essential for biological functions in living beings.<sup>20-22</sup> These analytes play an important role in maintaining the cardiovascular system, central nervous system functioning, enzyme regulation, gene expression, ion-transport mechanism, generation/bio-synthesis of neurotransmitters, DNA repairing etc. and therefore optimum concentration must be maintained in the body. These analytes can easily enter the human body through daily intake and their surplus concentration in the body may cause health complications such as high blood pressure, cellular damage, liver malfunctioning, Alzheimer's and Wilson's diseases, acute haemolytic anaemia, cerebral ischemia, amyotrophic lateral sclerosis etc.<sup>23, 24</sup> These analytes also play an irreplaceable role in electrical apparatus, food packaging, kitchenware manufacturing industries, which produce a huge amount of contaminated wastewater. Further, the discharge of untreated wastewater pollutes the waterbody ecosystem as these analytes are difficult to remove by traditional techniques of municipal water treatment plants.<sup>13, 25</sup>

To date, optical probes based on photo-physical mechanisms such as ICT, PET, CHEF, AIE, ESIPT etc. are extensively reported.<sup>26</sup> These probes mainly showed turn-on and turn-off of the fluorescence intensity. In the case of turn-on, the probe itself shows low fluorescence and once the analyte is introduced the fluorescence intensity increases. Whereas probes that exhibit high fluorescence (quantum yield), and the analyte addition decrease the fluorescence (quantum yield) are considered as turn-off probes. Among these, ESIPT-based probes are more promising due to their excellent photo-physical properties and multi-disciplinary applications.<sup>27, 28</sup> ESIPT process combines four stages of the photochemical process and involves the ground state and excited states of fluorophore isomers enol-form (E & E\*) and keto-form (K & K\*<sup>27</sup>). As depicted in scheme 1, on photoexcitation of fluorophore,

redistribution of electron takes place which elevates the H-bond donor group's acidity and acceptor group's basicity of Enol isomer, which allows photo-tautomerism with  $E^*$  to  $K^*$  conversion. Then,  $K^*$  comes to the K state by releasing energy as emission towards a higher wavelength than the emission wavelength of the enol form. Finally, fluorophore (K form) re-generates its original E form by reverse electron transfer. This four-staged process induces an unexpected high stokes shift ( $K^*$  to K conversion), which is uncommon with fluorophores which exhibit other photo-physical mechanisms. For developing ESIPT-based probes, researchers have used fluorophores namely, 2-(2'-hydroxyphenyl) benzimidazole(2-HBI)/ 2-(2'-hydroxyphenyl) benzoxazole(2-HBO)/ 2-(2'-hydroxyphenyl)benzothiazole (2-HBT), quinolines, flavones, quinoxalines etc. which consist H-bond donor ( $-NH_2$  and  $-OH$ ) and H-bond acceptor ( $-C=O/ =N-$ ) groups.<sup>29</sup>



**Scheme 1:** Schematic diagram for photophysical processes in ESIPT mechanism.

Recently, ESIPT-based probes have shown considerable development as optical sensors for biologically important analytes. A few excellent reviews have summarized the ESIPT-based probes for small analytes published till 2020.<sup>30-32</sup> Therefore, this review aims to summarize the ESIPT-based probes for anions, cations, and neutral species reported in the years 2021 & 2022. We have highlighted their structural design, photo-physical properties, mechanism of sensing, and potential applications. We believe this review will provide a timely overview of recent advances in ESIPT-based probes to researchers developing fluorescent probes for environmental and biological applications.

## ESIPT-based probes for Cations

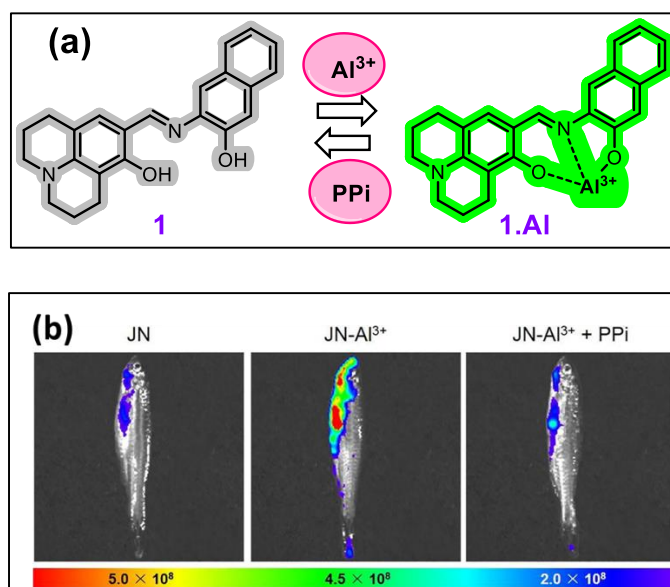


**Figure 1:** (a) Chemical structure of probe **1** and mechanism for PPI &  $\text{Al}^{3+}$  sensing. (b) Fluorescence images of zebrafish incubated with **1** (JN), **1**+  $\text{Al}^{3+}$  and **1**+ $\text{Al}^{3+}$ +PPI. Reproduced with permission from [33].

Xiao *et al.*<sup>33</sup> synthesized a julolidine derived Schiff base **1** for  $\text{Al}^{3+}$  and PPI (pyrophosphate) detection in  $\text{H}_2\text{O}/\text{DMSO}$  (v/v, 399/1). In  $\text{Al}^{3+}$  environment, fluorescence enhancement at 495 nm ( $\lambda_{\text{ex.}} = 450$  nm) and 520 nm (excimer formation) with excellent sensitivity (LOD=6.10 nM) was recorded. The spectral changes were attributed to synergistic effect of CHEF, PET, ICT, and ESIPT mechanisms which were confirmed by DFT (Density Functional Theory) calculations. Further, the **1**- $\text{Al}^{3+}$  ensemble was used for reversible sensing of PPI *via* the metal displacement approach. Along with the naked eye color change, **1** showed fluorescence change in adult zebrafish (Figure 1) and onion inner epidermal cells to detect  $\text{Al}^{3+}$  & PPI using fluorescence imaging experiments.

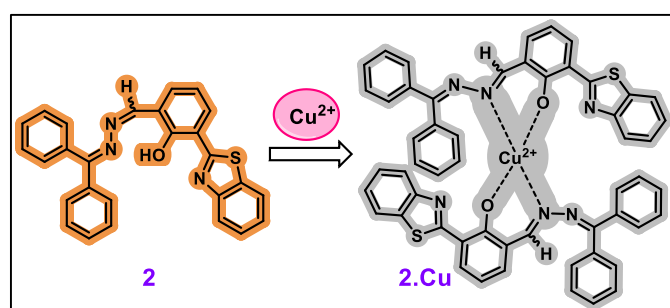


**Figure 2:** Chemical structure of probe **2** and detection mechanism to  $\text{Cu}^{2+}$ .

2-HBT is well-known for ESIPT properties and has been frequently used by researchers due to its easy synthesis and simpler structure. Using 2-HBT, Chatterjee *et al.*<sup>34</sup> synthesized a *turn-off* probe **2** for  $\text{Cu}^{2+}$  with colourless to yellow colour transformation in  $\text{DMF}-\text{H}_2\text{O}$  (1:9, v/v) medium. Probe **2** showed

excellent sensitivity towards  $\text{Cu}^{2+}$  which was supported by the LOD of 5 nM. The practical applications were explored by preparing probe **2** coated TLC plates for  $\text{Cu}^{2+}$  detection in solid-state and real samples collected from water bodies for  $\text{Cu}^{2+}$  quantification.

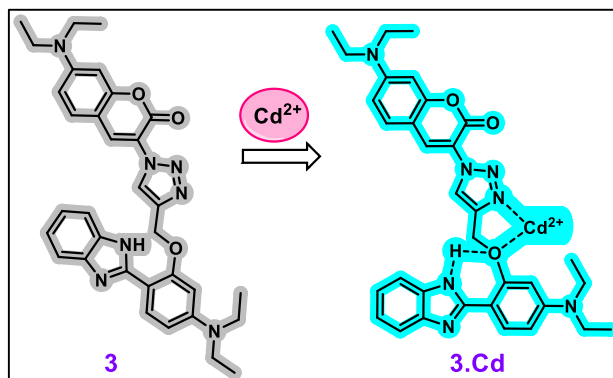


**Figure 3:** Chemical structure of probe **3** and detection mechanism to  $\text{Cd}^{2+}$ .

Using the copper-catalyzed azide-alkyne cycloaddition (CuAAC) approach<sup>35</sup>, Dey *et al.*<sup>36</sup> developed a highly selective  $\text{Cd}^{2+}$  probe **3** by connecting coumarin and benzimidazole units through a 1,2,3-triazole ring. With an LOD of 14 nM, probe **3** showed *turn-on* emission ( $\lambda_{\text{ex.}} = 380 \text{ nm}$ ,  $\lambda_{\text{em.}} = 485 \text{ nm}$ ) with  $\text{Cd}^{2+}$  in ACN solvent. Notably, probe **3** was found effective for  $\text{Cd}^{2+}$  detection in rat glial cells & human liver cells.

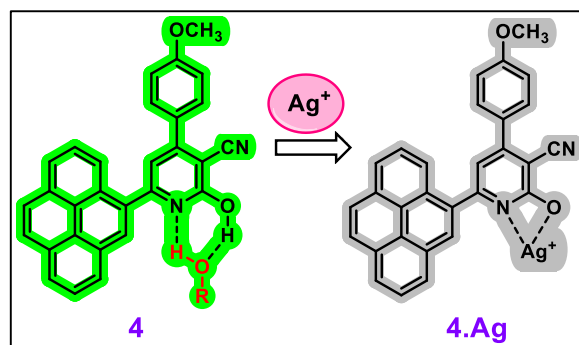


**Figure 4:** Chemical structure of probe **4** and detection mechanism to  $\text{Ag}^+$ .

Solvent-dependent ESIPT properties were exploited by Gong *et al.*<sup>37</sup> using pyrene-based *turn-off* probe **4** for  $\text{F}^-/\text{Ag}^+$  in EtOH/HEPES solution (3/1, 10.0  $\mu\text{M}$ , pH 7.2). In protic solvents, the keto fluorescence band of probe **4** was observed at 513 nm ( $\Phi = 0.896$ ), whereas in an aprotic solvent, the enol emission band showed at 450 nm. In UV-Vis, probe **4** showed absorbance spectra at 283 nm (enol form) and 385 nm (keto form). In the  $\text{F}^-$  environment, **4-F<sup>-</sup>** interaction undergoes H-bonding and induces the ratiometric emission change with quenching at 513 nm and increase at 450 nm. Similar spectral changes observed with  $\text{Ag}^+$  were attributed to chelation-induced quenching. The LOD with  $\text{F}^-$  and  $\text{Ag}^+$

was reported as 2.4 nM and 1.5 nM, respectively supporting the excellent sensitivity of probe **4**. Fluorescence cell imaging of **4** showed its application in monitoring the  $F^-$  and  $Ag^+$  in MCF-7 cells.

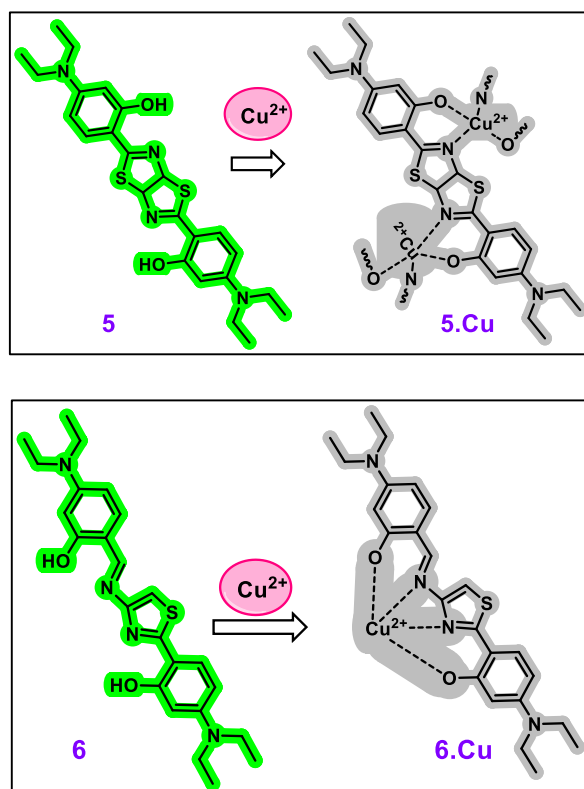


**Figure 5:** Chemical structure of probes **5** & **6** and their mechanism to  $Cu^{2+}$  sensing.

Madhu *et al.*<sup>38</sup> synthesized probes **5** & **6** for  $Cu^{2+}$  detection in ACN:water mixture. Probe **5** consists of two symmetrical thiazole rings fused together to provide  $\pi$ - $\pi$  stacking arrangement, whereas **6** is composed of a thiazole ring & Schiff base to give an unsymmetrical molecule with face-to-edge arrangements, which facilitate intramolecular H-bonding and ESIPt signal. In absorbance spectra of **5**, bands at 436 nm and 455 nm disappeared, and *in-situ* complex formation with  $Cu^{2+}$  give rise to a peak at 620 nm (LOD= 130 nM). In emission, the formation of **5.Cu**<sup>2+</sup> complex quenched the peak at 498 nm due to the paramagnetic effect. In the case of **6**, the 460 nm and 485 nm absorbance bands diminished, and with hypsochromic shift **6.Cu**<sup>2+</sup> exhibited absorbance at 388 nm. In emission, the peak at 520 nm was flattened and high sensitivity was observed and supported by calculated LOD as 10 nM for  $Cu^{2+}$ . Further, their applications as filter paper-based test strips were explored to support their utility in solid-state emission-based sensing.

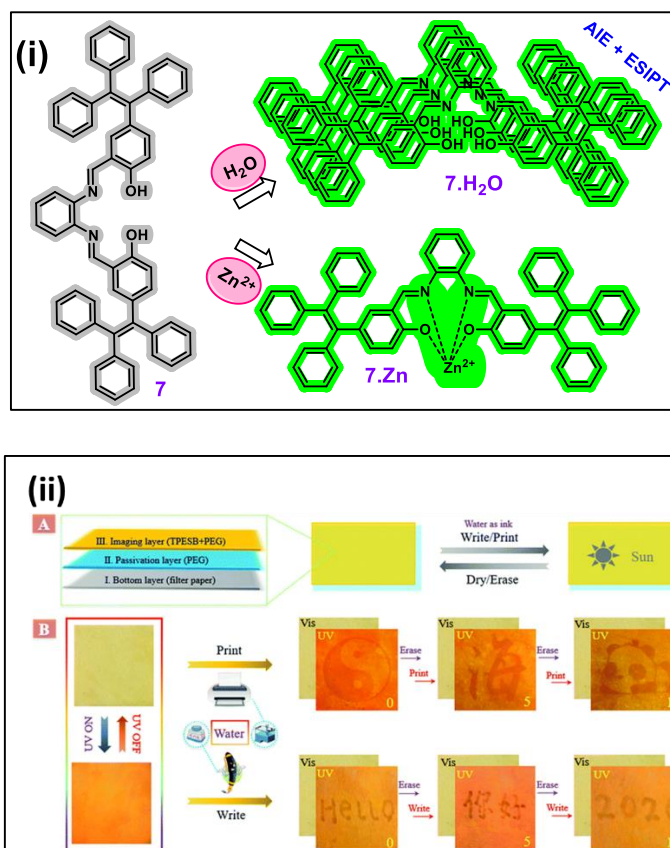


**Figure 6:** (i) Chemical structure of probe **7** and mechanism to water &  $Zn^{2+}$  sensing. (ii) Reversible ink-less writing using probe **7** coated filter paper using water as ink detectable (A) without and (B) with UV light. Reproduced from [39] © Royal Society of Chemistry.

Ni *et al.*<sup>39</sup> designed  $Zn^{2+}$  and water sensor **7** composed of tetraphenylethene unit and possess both AIE and ESIPT processes for detection. **7** induced red-shifted absorbance change (colourless to yellow) from 325 nm to a broad band at 400-500 nm range and showed fluorescence enhancement (bright yellow) at 590 nm in THF with 10 % water content. In the case of  $Zn^{2+}$ , similar absorbance enhancement (450 nm-500 nm) and emission spectra with naked eye colour changes were observed in THF: water (LOD = 38.9 nM). The formation of aggregates with water (AIE+ESIPT) and  $Zn^{2+}$  assisted chelation effect were responsible for the colour change and fluorescence change. Sensor **7** was successfully employed in developing inkless rewritable paper (Figure 6(ii)). Also, **7** showed low toxicity and was explored for application in  $Zn^{2+}$  detection in living cells through fluorescence cell imaging.

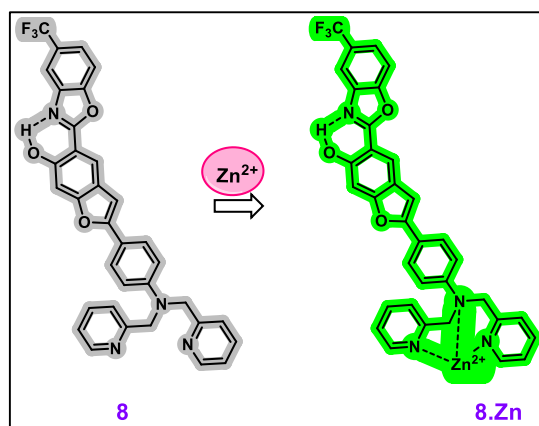


**Figure 7:** Chemical structure of probe **8** and mechanism to  $\text{Zn}^{2+}$  sensing.

Ulrich *et al.*<sup>40</sup> synthesized a  $\text{Zn}^{2+}$  sensor **8** with a di-picolylamine unit as the metal coordinating centre & 2-HBO as the ESIPY unit. Initially, **8** showed a fluorescence-on state which gets decreased at 480 nm ( $\text{E}^*$ ) and 576 nm ( $\text{K}^*$ ) with  $\text{Zn}^{2+}$  addition in DCM: ACN (9:1) mixture. The emission from  $\text{E}^*$  and  $\text{K}^*$  only, showed that the transient species exhibit no fluorescence and with 2:1 (**8**: $\text{Zn}^{2+}$ ) structure stoichiometry, supported by DFT calculations.

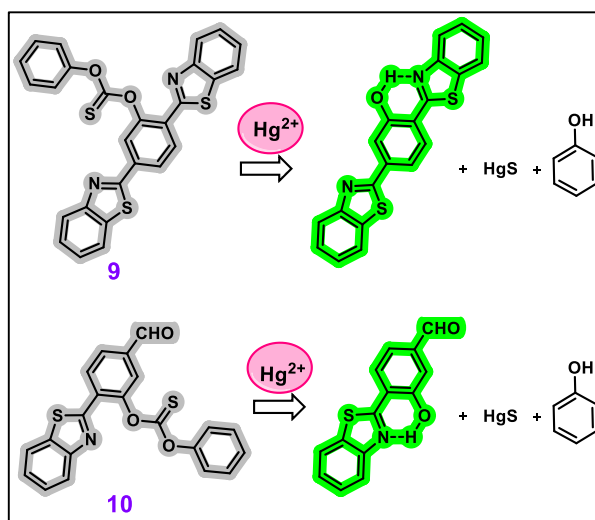


**Figure 8:** Chemical structure of probes **9** & **10** and mechanism for  $\text{Hg}^{2+}$  sensing.

Zheng *et al.*<sup>41</sup> developed two  $\text{Hg}^{2+}$  sensors **9** and **10** composed of thiocarbamate as  $\text{Hg}^{2+}$  binding sites. In the  $\text{Hg}^{2+}$  environment, emission spectra of **9** showed a peak diminishing at 405 nm and a new peak emerged at 525 nm (emission shift = 120 nm), whereas **10** showed an increase at 550 nm in HEPES: ACN (1:1, v/v).  $\text{Hg}^{2+}$ -assisted thiocarbamate group removal followed by restoration of the ESIPY process was responsible for spectral changes. The LOD for  $\text{Hg}^{2+}$  with **9** and **10** was calculated as  $0.31 \mu\text{M}$  and  $4.9 \mu\text{M}$ , respectively, with biological application to determine  $\text{Hg}^{2+}$  concentration in BSA and calf serum.



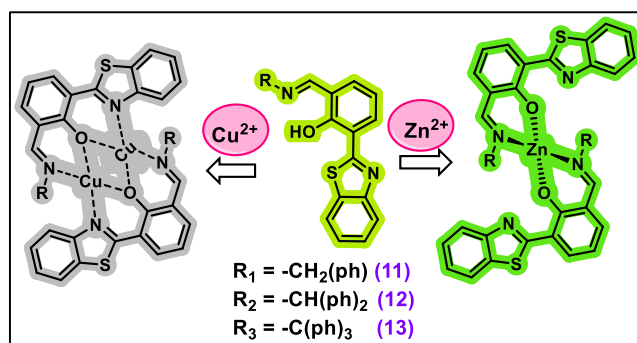


**Figure 9:** Chemical structure of probes **11**, **12** & **13** and sensing mechanism for  $\text{Cu}^{2+}$  &  $\text{Zn}^{2+}$ .

Zheng *et al.*<sup>42</sup> synthesized three probes **11**, **12** and **13** based on the benzothiazole unit with dual AIE-ESIPT mechanisms for *turn-on* detection of  $\text{Zn}^{2+}$  and *turn-off* detection of paramagnetic  $\text{Cu}^{2+}$ , respectively. In emission, **11** and **12** showed an emission decrease at 535 nm ( $\lambda_{\text{ex.}} = 435$  nm) with  $\text{Cu}^{2+}$  with LOD of 0.774  $\mu\text{M}$  and 1.35  $\mu\text{M}$ , respectively, in THF/HEPES (3:7, v/v, pH = 7.4). Interestingly, **11**, **12** and **13** behaved as *turn-on* sensors for  $\text{Zn}^{2+}$  in EtOH/HEPES (9: 1, v/v, pH = 7.4). For **11**, a blue-shifted ratiometric change from 520 nm (weak emission) to 470 nm (strong emission) with  $\text{Zn}^{2+}$  (LOD= 0.911  $\mu\text{M}$ ) at  $\lambda_{\text{ex.}} = 400$  nm. For **12**, a similar pattern was observed with blue-shifted emission from 557 nm to 480 nm with a LOD of 1.01  $\mu\text{M}$ , and for **13**, only a slight enhancement in emission at 470 nm was recorded with  $\text{Zn}^{2+}$ . The strong fluorescence was utilised for  $\text{Zn}^{2+}$  and  $\text{Cu}^{2+}$  detection using test paper strips. Overall, **11** and **12** showed better selectivity and overall enhancement compared to **13**. Whereas **11** showed better LOD compared to **12** for both  $\text{Cu}^{2+}$  and  $\text{Zn}^{2+}$  ions.

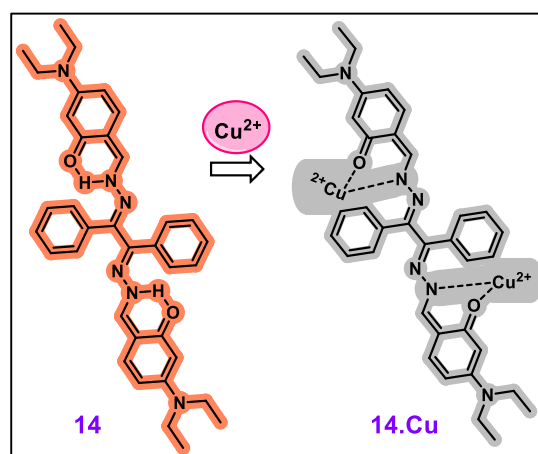


**Figure 10:** Chemical structure of probe **14** and mechanism for  $\text{Cu}^{2+}$  sensing.

A *turn-off* fluorescent probe **14** for  $\text{Cu}^{2+}$  was developed by Zhu *et al.*<sup>43</sup>, with absorption bands at 267 nm, 409 nm, and 492 nm. The absorption at 409 nm was attributed to n- $\pi^*$  transition and 492 nm to the keto-tautomer. With a Stokes shift of 159 nm, new emission was recorded at 568 nm ( $\Phi = 0.13$ ) and can detect  $\text{Cu}^{2+}$  as low as 0.2  $\mu\text{M}$  in THF/ $\text{H}_2\text{O}$  ((v/v), 1:1, pH = 7.4). Also, **14** showed solid-state photo-

physical properties with absorbance and emission peaks at 413 nm & 537 nm, respectively, and were further exploited for the test strip-based  $\text{Cu}^{2+}$  detection as a practical application.

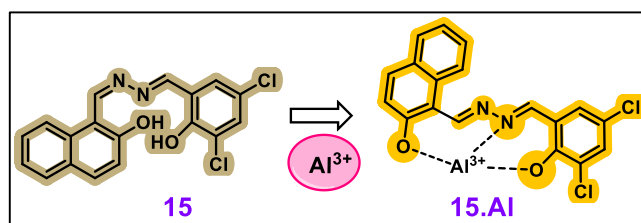


**Figure 11:** Chemical structure of probe **15** and mechanism for  $\text{Al}^{3+}$  sensing.

Anshori *et al.*<sup>44</sup> synthesized a 2-hydroxynaphthaldehyde-derived *turn-on* sensor **15** for  $\text{Al}^{3+}$  with two imine groups. Probe **15** exhibited good selectivity, reversibility and a high quantum yield of 0.203 with  $\text{Al}^{3+}$  in DMSO:  $\text{H}_2\text{O}$ (99:1,v/v) and can detect  $\text{Al}^{3+}$  with a minimum concentration of 0.04  $\mu\text{M}$  at 546 nm ( $\lambda_{\text{ex.}}=360\text{nm}$ ). The ESIPT inhibition was observed due to the complex formation with  $\text{Al}^{3+}$ .

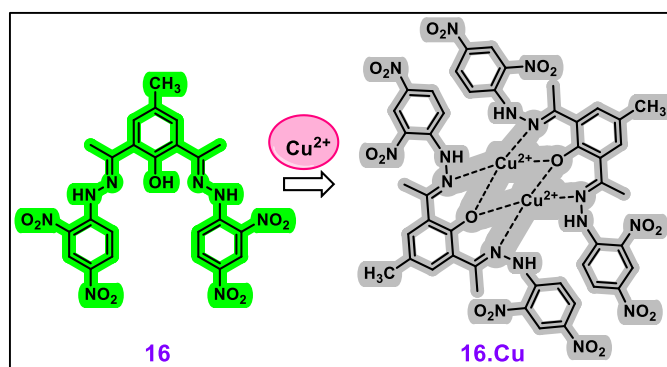


**Figure 12:** Schematic representation of probe **16** for  $\text{Cu}^{2+}$  sensing.

A hydrazine-based colourimetric and fluorescent sensor **16** was synthesized by Arabahmadi<sup>45</sup> for  $\text{Cu}^{2+}$  and  $\text{F}^-$  detection in DMSO solvent. In  $\text{F}^-$  environment, the initial absorbance at 390 nm and 490 nm decreased, and a colour change (red to purple) showed red shift to 513 nm. The ICT mechanism between  $-\text{OH}/-\text{NH}$  sites and EWG ( $-\text{NO}_2$ ) was responsible for the spectral shift. In emission, low fluorescence ( $\Phi = 0.105$ ) was recorded due to the existing PET process from the nitrogen lone pair of the imine group to the 4-methyl phenol unit, which showed enhancement at 532 nm ( $\lambda_{\text{ex.}}=490\text{ nm}$ ,  $\Phi = 0.56$ ,  $\text{LOD}=3.26\ \mu\text{M}$ ) with  $\text{F}^-$  addition. In  $\text{Cu}^{2+}$  co-existence, a decrease at 490 nm and enhancement at 400 nm (red to yellow colour change) was observed in absorbance spectra. Whereas a decrease in emission intensity at 532 nm was recorded with  $\text{Cu}^{2+}$  ( $\text{LOD}=3.51\ \mu\text{M}$ ), and practical applications were explored by constructing different logic gates with  $\text{Cu}^{2+}$  and  $\text{F}^-$  as inputs and paper strips for colorimetric detection.

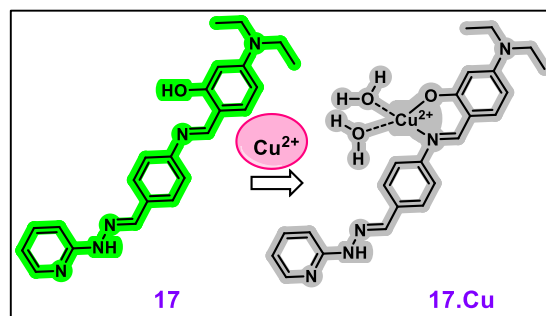


**Figure 13:** Chemical structure of probe **17** and mechanism for  $\text{Cu}^{2+}$  sensing.

Chansaenpak *et al.*<sup>46</sup> synthesized  $\text{Cu}^{2+}$  probe **17** with salicylideneaniline as a metal coordination site. With  $\text{Cu}^{2+}$ , both absorbance band at 440 nm (bright pale to light yellow) and emission peak and 510 nm ( $\lambda_{\text{ex.}} = 430$  nm) diminished. Probe **17** can selectively detect  $\text{Cu}^{2+}$  of concentration 0.87 ppb in  $\text{H}_2\text{O}/\text{CH}_3\text{CN}$  (9:1, v/v). Further, biological application was explored by live cell imaging experiments to detect  $\text{Cu}^{2+}$  in live U251 cells.

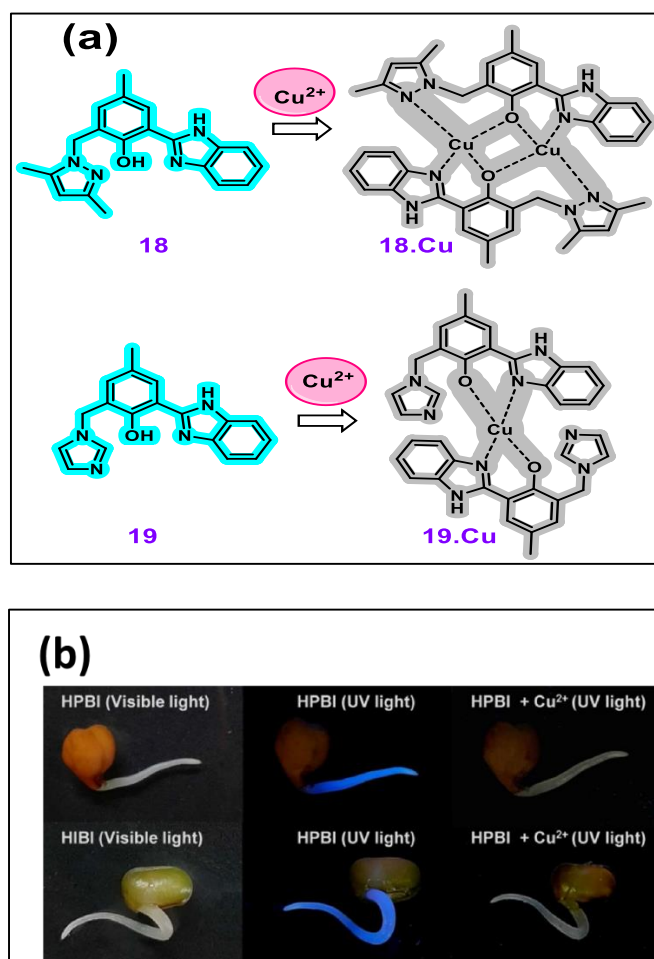


**Figure 14:** (a) Chemical structure of probes **18** (HPBI) & **19** (HIBI) and mechanism for  $\text{Cu}^{2+}$  sensing. (b) Chickpea (top) incubated with **18** and Mung bean sprouts (below) incubated with **19** followed by  $\text{Cu}^{2+}$  solution. Reproduced with permission from [47].

Goswami *et al.*<sup>47</sup> developed 2-HBI moiety-based *turn-off* probes **18** and **19** for Cu<sup>2+</sup> with good sensitivity (LOD = 28.5 nM for **18** and 4.22 nM for **19**) in Ethanol: HEPES–buffer solution (v/v, 1: 9, pH = 7.4). With excitation at 326 nm, **18** exhibited strong ESIPT emission ( $\Phi = 0.237$ ) at 474 nm, whereas **19** showed strong emission ( $\Phi = 0.241$ ) at 471 nm, when excited at 328 nm. Also, **18** and **19** showed decreases in emission intensity in the Cu<sup>2+</sup> environment with good selectivity. Both **18** and **19** displayed good bio-compatibility and rapid sensing of intracellular Cu<sup>2+</sup> by quenching fluorescence. Furthermore, **18** and **19** showed fluorescence decrease with Cu<sup>2+</sup> in MCF–7 cells, and sprouted food grains (Figure 14b).

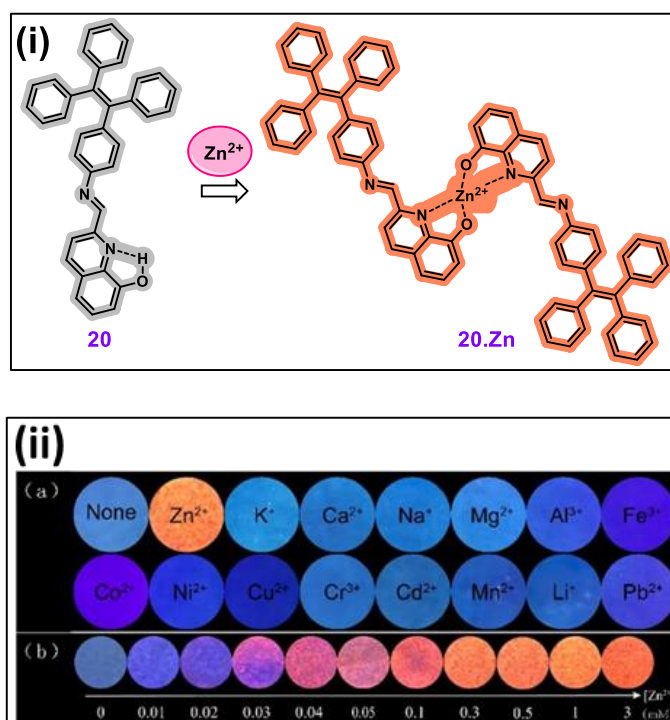


**Figure 15:** (i) Chemical structure of probe **20** and mechanism for Zn<sup>2+</sup> sensing. (ii) Photograph images of filter-paper-based test strips coated with probe **20** and their response to (a) metal ions and (b) various concentration of Zn<sup>2+</sup>. Reproduced from [48].

Ma *et al.*<sup>48</sup> synthesized D– $\pi$ –A type probe **20** for Zn<sup>2+</sup> sensing with ESIPT-active and acceptor 8-hydroxyquinoline group and TPE group as electron donor group. In THF: water medium, Zn<sup>2+</sup> exhibited fluorescence enhancement at 596 nm ( $\lambda_{\text{ex.}} = 420$  nm) due to ESIPT-AIE “on” state. The involvement of the AIE process was confirmed by DLS studies, and the ESIPT process was confirmed by theoretical calculations. Further, as shown in figure 15(ii), paper test strips were fabricated utilizing ESIPT-AIE coupled naked eye detectable fluorescence change selectively with Zn<sup>2+</sup>.

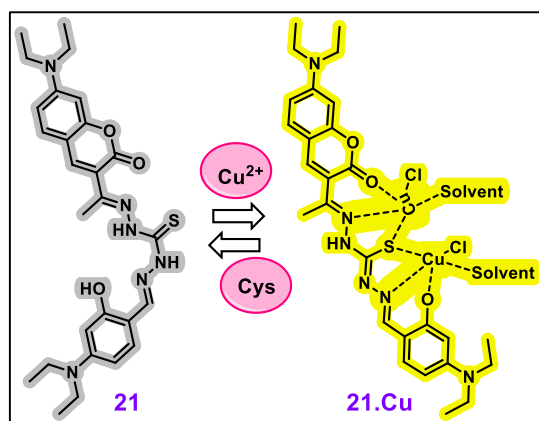


**Figure 16:** Schematic representation of probe **21** for  $\text{Cu}^{2+}$  & Cys sensing.

Murugesapandian *et al.*<sup>49</sup> developed coumarin-derived unsymmetrical thiocarbohyrazone **21** for moisture,  $\text{Cu}^{2+}$  and Cys sensing. The moisture detection was based on the  $\text{F}^-$  assisted deprotonation of phenol and thiourea amide unit in DMF solvent to give yellow to orange colour change and red-shifted absorbance from 380 nm to 396 nm. In emission, the addition of water quenched the peak at 525 nm ( $\lambda_{\text{ex.}} = 380$  nm) and a peak formed in the 565 - 630 nm region. For cation sensing,  $\text{Cu}^{2+}$  addition to **21** triggered a bathochromic-shifted absorbance from 380 nm to 475 nm in DMF/ $\text{H}_2\text{O}$  (9:1, v/v; Tris-HCl, pH= 7.2). Interestingly, the faintly emissive peaks at 435 nm and 525 nm displayed selective enhancement with  $\text{Cu}^{2+}$  at 455 nm due to ESIPT off state. Further, the **21**- $\text{Cu}^{2+}$  complex was employed for Cys detection, which showed reversible spectral changes recorded with  $\text{Cu}^{2+}$  (LOD = 68 nM). Further, reversible changes with Cys were observed due to metal displacement reaction with a LOD of 2.33  $\mu\text{M}$ . The application of **21** was explored by constructing logic gates and paper strips for  $\text{Cu}^{2+}$  and Cys detection.

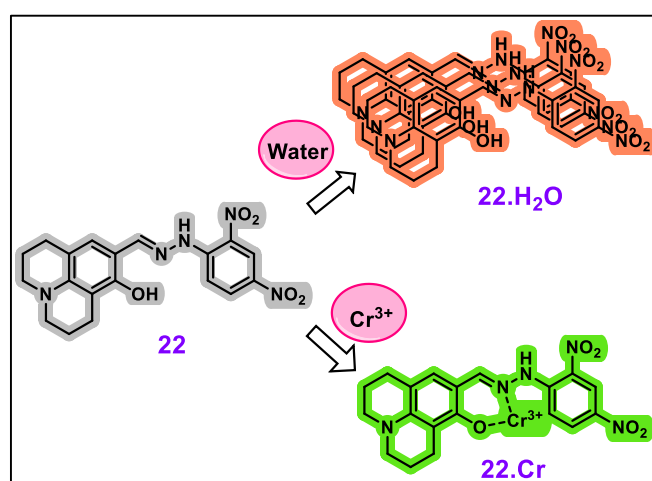


**Figure 17:** Schematic representation of probe **22** for  $\text{Cr}^{3+}$  & moisture sensing.

Jose *et al.*<sup>50</sup> synthesized a multianalyte probe **22** for the detection of  $\text{Cr}^{3+}$ , arsenate( $\text{HAsO}_4^{2-}$ ) and PPI in a DMSO-water medium. Probe **22** also showed AIE properties which were confirmed by recording emission spectra with different water fractions. In DMSO:water(4:1, v/v) mixture, the initial weak monomer emission of **22** displayed significant enhancement with  $\text{Cr}^{3+}$  at 420 nm(enol) and a decrease in keto peak at 585 nm( $\lambda_{\text{ex.}}=365$  nm) due to complex formation and *ESIPT-off* state. In anion sensing studies, **22** displaced spectral changes with arsenate and PPI anions with a hypsochromic emission shift from 585 nm to 510 nm. In Uv-vis, PPI showed more spectral and colour change than arsenate ion. However, PPI showed more enhancement in emission than arsenate ion. The LOD for  $\text{Cr}^{3+}$ , arsenate and PPI was reported as  $3.9 \mu\text{M}$ ,  $3.9 \mu\text{M}$  and  $0.19 \mu\text{M}$ , respectively.

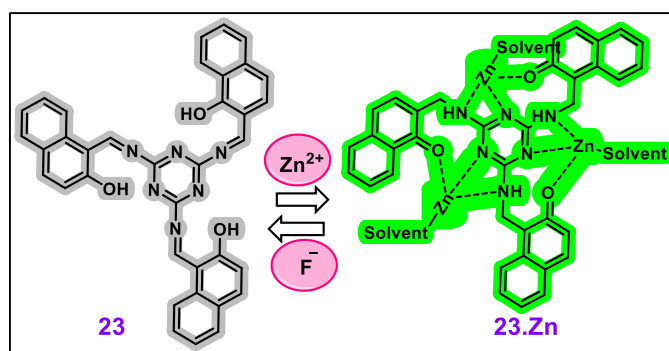


**Figure 18:** Schematic representation of probe **21** for  $\text{Zn}^{2+}$  &  $\text{F}^-$  sensing.

Uahengo *et al.*<sup>51</sup> constructed a multianalyte sensor **23** which displayed colourimetric response with cations ( $\text{Zn}^{2+}$ ,  $\text{Co}^{2+}$ ,  $\text{Ni}^{2+}$  and  $\text{Cu}^{2+}$ ) and selectively triggered fluorescence increase with  $\text{Zn}^{2+}$  in acetonitrile solvent. Initially, probe **23** exhibited fluorescence peaks at 483 nm and 510 nm merged due to coordination with  $\text{Zn}^{2+}$  and centred at 493 nm, and the ICT mechanism was responsible for *turn-on* response. Further, **23** showed reversible properties with  $\text{F}^-$  addition due to the metal displacement reaction and restoration of the non-complex structure.

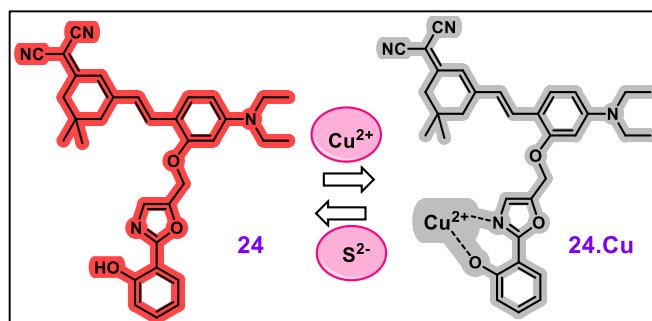


**Figure 19:** Chemical structure of probe **24** and mechanism for  $\text{Cu}^{2+}$  sensing.

As a sequential probe for  $\text{Cu}^{2+}$  and  $\text{S}^{2-}$ , Xu *et al.*<sup>52</sup> reported an oxazole-based NIR absorbing probe **24** with fluorescence at 690 nm( $\lambda_{\text{ex.}}=510$  nm) in DMSO-HEPES buffer. In the  $\text{Cu}^{2+}$  environment, **24**

showed *turn-off* emission (ESIPT-*off*) with good selectivity. Further, the **24**.Cu<sup>2+</sup> ensemble employed for S<sup>2-</sup> detection via metal displacement approach. In S<sup>2-</sup>, reversible spectral change with fluorescence increment was observed at 690 nm. Further, probe **24** was employed to detect Cu<sup>2+</sup> and S<sup>2-</sup> in live cells with emission in the NIR region.

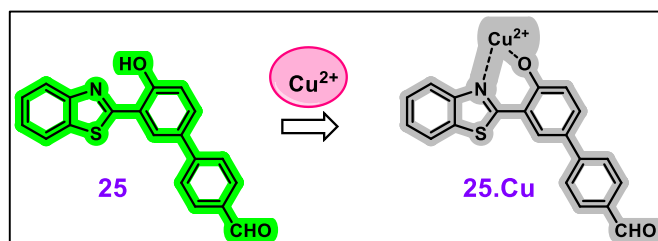


**Figure 20:** Schematic representation of probe **25** for Cu<sup>2+</sup> sensing.

Singh *et al.*<sup>53</sup> synthesized 2-HBT-derived *turn-off* probe **25** for Cu<sup>+</sup> and Cu<sup>2+</sup> with LOD of 69 nM and 250 nM, respectively in HEPES buffer–CH<sub>3</sub>CN (9:1, v/v, pH 7.2). Probe **25** showed high fluorescence due to combined AIE-ESIPT photo-physical mechanisms. In the Cu species (Cu<sup>+</sup> and Cu<sup>2+</sup>), the complex formation with O and N atoms of the hydroxybenzothiazole unit blocked the ESIPT and prevented the formation of aggregates. Thereby, fluorescence quenching was recorded at 520 nm ( $\lambda_{\text{ex.}} = 360$  nm). Further, probe **25** was utilised for Cu<sup>2+</sup> detection in real samples, live-cell imaging in A549 cells, anti-cancer activity in HeLa cell and MG63 cell lines, probe-coated filter paper strips, TLC strip-based detection and inkless-writing confirmed the interdisciplinary applications of **25**.

## ESIPT based probes for Anions

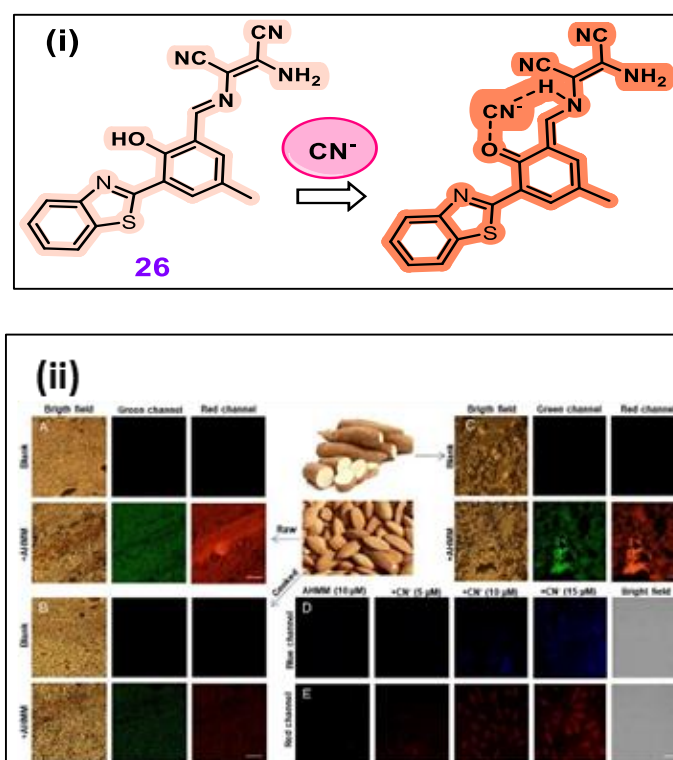


**Figure 21:** (i) Schematic representation of probe **26** (AHMM) for CN<sup>-</sup> sensing. (ii) fluorescence imaging of probe **26** with raw almond, cooked almond, and cassava. Fluorescence imaging of probe **26** and different concentrations of CN<sup>-</sup>. Reproduced from [54]

Qiao *et al.*<sup>54</sup> synthesized CN<sup>-</sup> probe **26** having H-bonding for ESIPT process with good selectivity in DMSO/H<sub>2</sub>O (8/2, v/v). Probe **26** showed a Stokes shift of 225 nm with excellent sensitivity and LOD of  $4.47 \times 10^{-8}$  M. Further, **26** was utilised to explore potential applications for CN<sup>-</sup> detection in tap water, the smartphone app for on-field quantification of CN<sup>-</sup>, fluorescence imaging in almonds and cassava (figure 21(ii)), and biological applications as imaging in cells and mice.

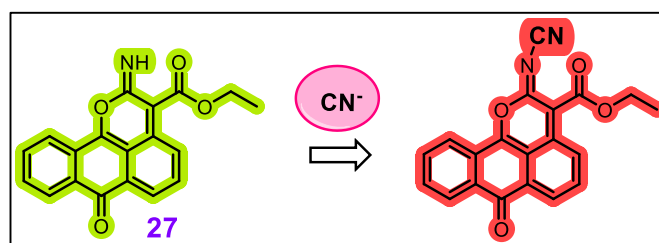


**Figure 22:** Schematic representation of probe **27** for CN<sup>-</sup> sensing.

With excellent selectivity, Liu *et al.*<sup>55</sup> developed an imine-based colorimetric and fluorogenic probe **27** for CN<sup>-</sup>. In the CN<sup>-</sup> environment, -NH deprotonation disturbed the intramolecular H-bonding and thereby displayed ratiometric UV-vis change at 443nm (decrease) and 517 nm (increase) with yellow



to pink in CH<sub>3</sub>CN/H<sub>2</sub>O mixture. The LOD for CN<sup>-</sup> was calculated as 13.06  $\mu$ M with fluorescence changes at 477 nm (decrease) and 733 nm (increase). Furthermore, probe **27** was utilised for the cyanide detection in cassava flour and bitter almonds.

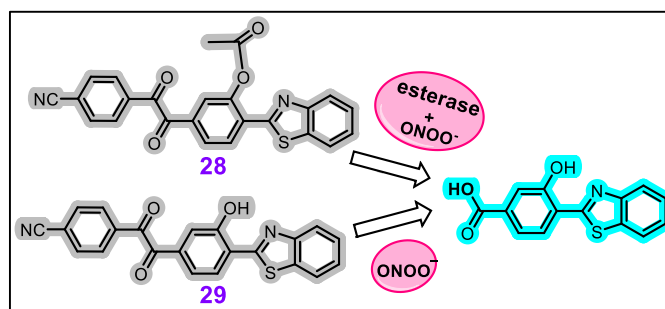


**Figure 23:** Schematic representation of probes **28** & **29** for ONOO<sup>-</sup> sensing.

Dong *et al.*<sup>56</sup> reported *turn-off* fluorescent probes **28** and **29** for ONOO<sup>-</sup> based on dual PET-ESIPT mechanisms in PBS buffer (10 mM, 10% MeOH, pH 7.4). The emission of probe **29** enhanced at 490 nm ( $\lambda_{\text{ex.}} = 405$  nm) with a large Stokes shift of 135 nm (absorbance peak at 365 nm) and LOD was reported as 36 nM. In the case of **29**, similar absorbance and emission changes were recorded only in the esterase environment due to the hydrolysis of the ester group. Further, imaging of ONOO<sup>-</sup> in live cells, zebra fish model and the brain of depressive mouse confirmed the biological utility of **28** & **29**.

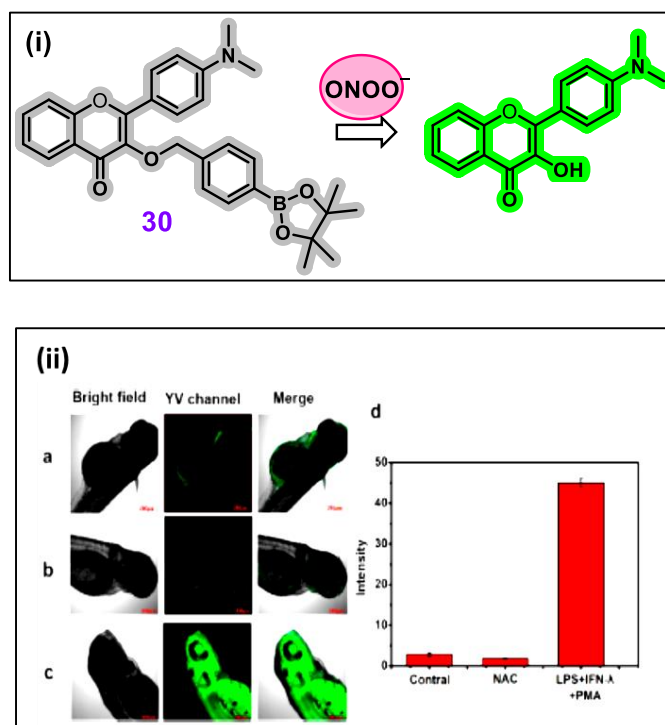


**Figure 24:** (i) Schematic representation of probe **30** for ONOO<sup>-</sup> sensing. (ii) (a) Fluorescence imaging of zebrafish treated with **30**, (b) zebrafish pre-treated with NAC and **30**. (c) Zebrafish pretreated with LPS and IFN- $\gamma$  followed by incubation in PMA and probe **30**. (d) Statistical representation of observed fluorescence intensity. Reproduced by permission from [57]

To detect  $\text{ONOO}^-$ , Jing *et al.*<sup>57</sup> synthesized probe **30**, which can undergo  $\text{ONOO}^-$  triggered dissociation of the boronic ester, releasing flavonoid fluorophore and *ESIPT-on* state in PBS buffer. The dissociation of boronic ester-induced red shift in emission peak with high selectivity, stokes shift of 140 nm and LOD of 17.3 nM. Probe **30** showed bio-compatibility which was confirmed by  $\text{ONOO}^-$  visualization via fluorescence imaging in HeLa cells and zebrafish.

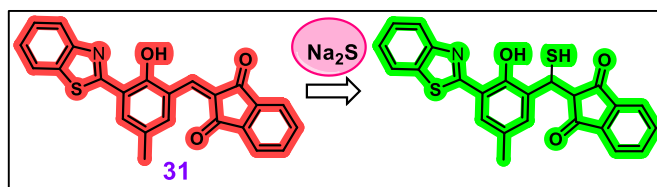


**Figure 25:** Schematic representation of probe **31** for  $\text{H}_2\text{S}$  sensing.

Du *et al.*<sup>58</sup> reported probe **31** for  $\text{H}_2\text{S}$  which showed spectral changes by undergoing nucleophilic addition reaction in  $\text{CH}_3\text{CN}$ :  $\text{PBS}(1:1, \text{v/v}, \text{pH} = 7.4)$ . In  $\text{H}_2\text{S}$ , probe **31** exhibited blue-shifted emission from 630 nm to 542 nm (stokes shift= 240 nm) with red-to-green emission transformation. Whereas, the Uv-vis band at 577 nm diminished and enhancement was observed at 445 nm, selectivity with  $\text{H}_2\text{S}$ . Probe **31** was also explored for monitoring endogenous and exogenous  $\text{H}_2\text{S}$  in cells and  $\text{H}_2\text{S}$  fluctuation in both *in-vitro* and *in-vivo*.

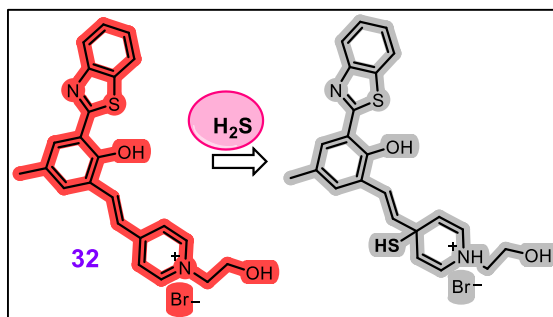


**Figure 26:** Schematic representation of probe **32** for  $\text{H}_2\text{S}$  sensing.

The same research group<sup>59</sup> also synthesized 2-HBT derived NIR absorbing derived mitochondria-targeted  $\text{H}_2\text{S}$  probe **32**. Using the same sensing mechanism as used in **31**,  $\text{H}_2\text{S}$  addition to **32** induced a hypsochromic shift ( $\sim 188$  nm) in emission from 658 nm (keto) to 470 nm (enol) in  $\text{PBS}/\text{CH}_3\text{CN}$  buffer (1/1, v/v,  $\text{pH} = 7.4$ ). Further, quick response and good selectivity are other advantages of **32**. The excellent biocompatibility and mitochondrial targeting ability of **32** due to the pyridinium group were confirmed by monitoring mitochondrial  $\text{H}_2\text{S}$  in HepG2 cells.

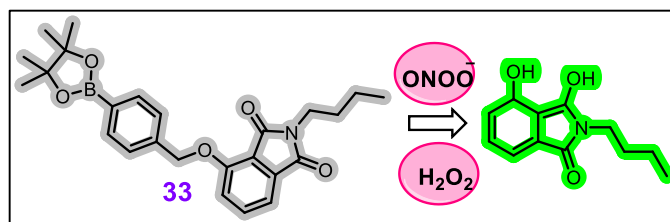


**Figure 27:** Schematic representation of probe **33** for  $\text{ONOO}^-/\text{H}_2\text{O}_2$  sensing.

James *et al.*<sup>60</sup> reported probe **33** for  $\text{ONOO}^-$  probe with ESIPT off state due to the phenylboronic acid pinacol ester group. The boronic ester group gets cleaved with the addition of  $\text{ONOO}^-/\text{H}_2\text{O}_2$ , and subsequent ESIPT *on* was observed with enhanced fluorescence in PBS buffer solution (10 mM, pH = 7.4). Kinetic studies confirmed higher reactivity of more nucleophilic  $\text{ONOO}^-$  than  $\text{H}_2\text{O}_2$ . Probe **33** was explored for endogenous  $\text{ONOO}^-$  visualization in HeLa cells under physiological conditions. Furthermore, two-photon excitation at 750 nm was applied to detect exogenous  $\text{ONOO}^-$  even at depth of 110  $\mu\text{m}$  in rat hippocampal slices.

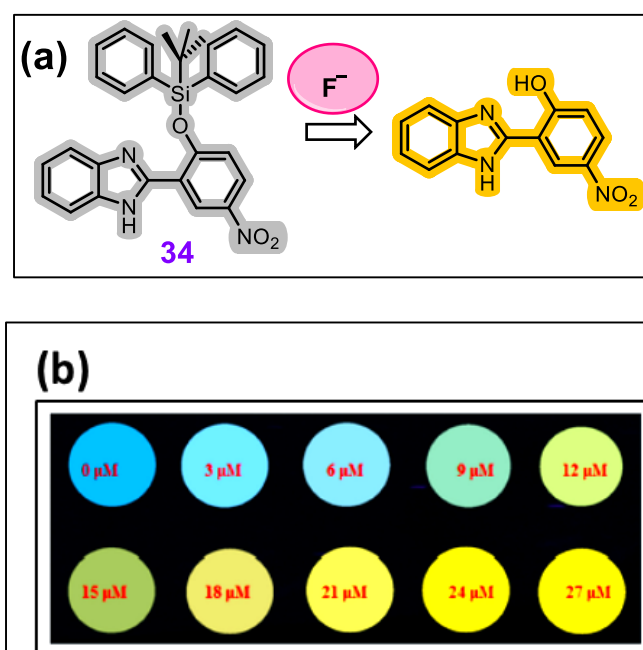


**Figure 28:** (a) Chemical structure of probe **34** and mechanism for  $\text{F}^-$  sensing. (b) Naked eye detectable color change in fluorescence of filter paper strip coated with probe **34** with the increasing amount of  $\text{F}^-$ . Reproduced by permission from [61]

Utilizing smartphone as a portable device for detection, Nie *et al.*<sup>61</sup> synthesized a fluoride sensor **34** based on the silyl-derived benzimidazole unit. The addition of  $\text{F}^-$  cleaved the Si-O bond and thereby induced ESIPT *on* state with the diminished emission at 437 nm (enol), and a peak emerged at 550 nm ( $\lambda_{\text{ex.}} = 347 \text{ nm}$ ) in THF/ $\text{H}_2\text{O}$  (9:1, v/v). High selectivity and good LOD for  $\text{F}^-$  as 0.11  $\mu\text{M}$  were

advantageous for real applications. Further, blue to yellow naked-eye detectable fluorescence (Figure 28b) was exploited for smartphone-assisted  $F^-$  detection in groundwater samples.

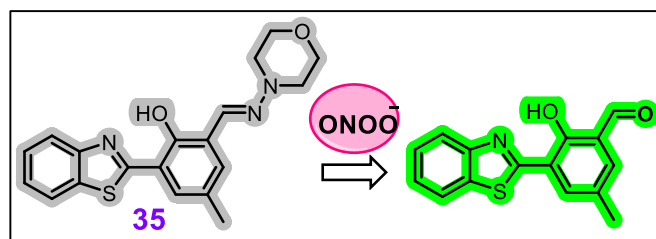


**Figure 29:** Chemical structure of probe **35** and mechanism for  $ONOO^-$  sensing.

Shen *et al.*<sup>62</sup> designed a benzothiazole-derived sensor **35** for selective detection of  $ONOO^-$  with excellent bio-compatible properties due to the presence of lysosome targeted morpholine unit. Probe **35** showed a selective and quick emission increment of 83-fold at 515 nm, with colourless to yellow color transformation due to  $ONOO^-$  reaction with morpholine hydrazine in PBS buffer: DMSO (9:1, pH 7.4). The biological application and lysosomal targeting ability of **35** were confirmed by fluorescence cell imaging and co-localization experiments with HeLa cells.

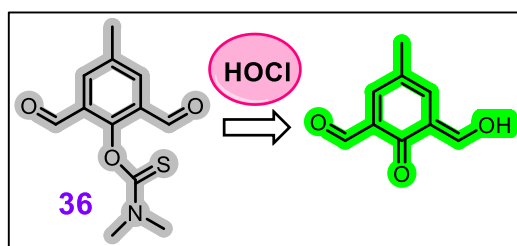


**Figure 30:** Schematic representation of probe **36** for  $ClO^-$  sensing.

Wang *et al.*<sup>63</sup> designed probe **36** with combined AIE and ESIPT mechanisms for fast and selective sensing and imaging  $HOCl$  ( $ClO^-$ ). In the  $HOCl$  environment, the dimethylthiocarbamate group removal from **36** gives ESIPT and AIE “on” state (free -OH group) with 110-fold emission heightening at 535 nm ( $\lambda_{ex.} = 430$  nm) in PBS buffer. The fluorescence change was also recorded by monitoring endogenous and exogenous  $HOCl$  in RAW264.7 cells and the zebrafish model.

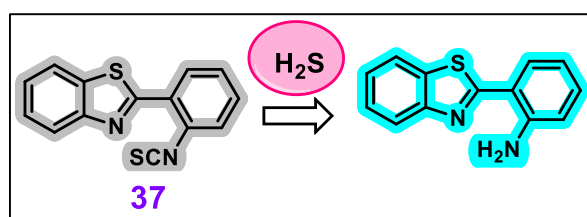


**Figure 31:** Schematic representation of probe **37** for  $H_2S$  sensing.

Jang *et al.*<sup>64</sup> reported a 2-(2-aminophenyl) benzothiazole-based sensor **37** for H<sub>2</sub>S (S<sup>2-</sup>) with high selectivity. The HBT fluorophore was derived with electron-withdrawing isothiocyanate moiety, which gets converted to –NH<sub>2</sub> group by H<sub>2</sub>S and subsequently restoring the ESIPT with enhanced emission at 447 nm ( $\lambda_{\text{ex.}} = 309$  nm) in DMF:HEPES (7:3, v/v, pH 7.4). In UV-vis, ratiometric response with band increase at 373 nm and decrease at 309 nm was recorded with H<sub>2</sub>S. The LOD of probe **37** for S<sup>2-</sup> was reported as 91.7 nM, and application was explored using confocal microscopy by detecting H<sub>2</sub>S in HeLa cells.

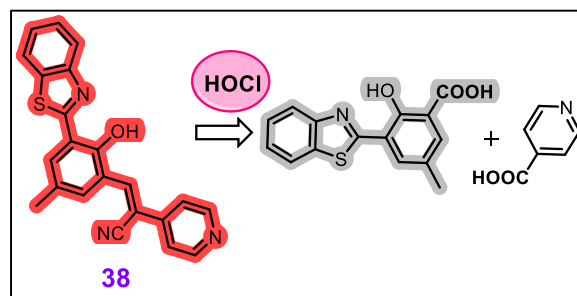


**Figure 32:** Schematic representation of probe **38** for HOCl sensing.

Yin *et al.*<sup>65</sup> synthesized a *turn-off* sensor **38** for HOCl (ClO<sup>-</sup>) derived from 2-HBT moiety. In the initial state ( $\lambda_{\text{ex.}} = 400$  nm, stokes shift= 207 nm), dual fluorescence peaks were recorded at 469 nm and 607 nm in PBS:ACN (7:3, v/v, pH 7.4). The HOCl addition triggered oxidation reaction in **38** and induced the *ESIPT-off* state due to the electron-withdrawing free carboxylate groups within 26 seconds. The keto emission reduced to one-fifth of the initial intensity at 607 nm, and a *turn-off* response was also observed in the cell imaging experiments with HeLa cells for biological applications.

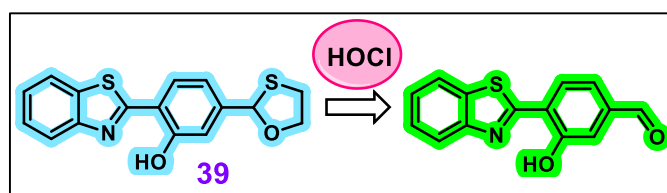


**Figure 33:** Schematic representation of probe **39** for HOCl sensing.

With high selectivity and quick *turn-on* response, Fang *et al.*<sup>66</sup> developed probe **39** for the HClO<sup>-</sup>/ClO<sup>-</sup>. 1,3-oxathiolane used as the responsive group for HClO<sup>-</sup>/ClO<sup>-</sup>, whereas 2-HBT acts as the signalling unit. Probe **39** showed ratiometric emission change at 461 nm (decrease) and 555 nm (increase) with good sensitivity for HClO<sup>-</sup>/ClO<sup>-</sup> (LOD = 2.03 x 10<sup>-6</sup> M) and high selectivity among common anions and cations in PBS:ACN (9:1, v/v, pH 7.4)..

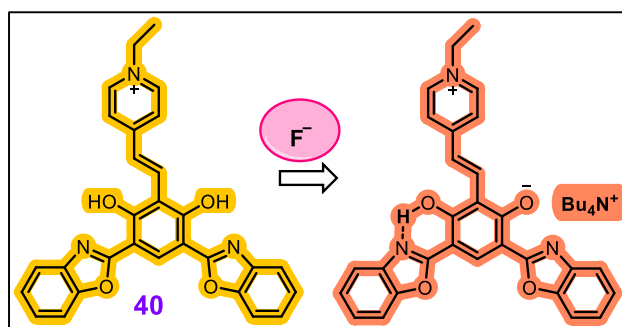


**Figure 34:** Schematic representation of probe **40** for  $F^-$  sensing.

Pang *et al.*<sup>67</sup> synthesized benzoxazole-based NIR absorbing probe **40** for  $F^-$  with initial emission at 605 nm ( $\lambda_{ex.} = 380$  nm) due to ICT and enol emission in acetonitrile solvent. The  $F^-$  removed the phenolic protons due to the deprotonation reaction and showed an absorbance shift from 390 nm to 535 nm (light yellow to purple colour change). Also, in emission, probe **40** showed peak enhancement at 720 nm ( $\lambda_{ex.} = 535$  nm) with  $F^-$  attributed to keto emission due to ESIPT “on” state.

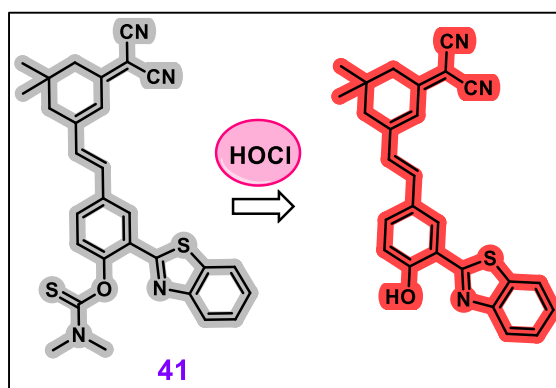


**Figure 35:** Schematic representation of probe **41** for HOCl sensing.

Chen *et al.*<sup>68</sup> synthesized NIR probe **41** for HOCl( $ClO^-$ ) using the dicyanoisophorone and benzothiazole unit with dimethyl thiocarbamoyl chloride blocked -OH group and thereby ESIPT and ICT-off state ( $\Phi = 0.0011$ ). The introduction of HOCl triggered the release of the HBT unit and restored the ESIPT and ICT processes with the emission increment recorded at 700 nm ( $\lambda_{ex.} = 520$  nm,  $\Phi = 0.141$ ) in EtOH:PBS (1:1, v/v, pH 7.4). The HOCl showed high sensitivity with a quick response of 3 seconds and 4.04 nM. The biocompatibility of **41** was confirmed by endogenous and exogenous HOCl imaging in live cells.

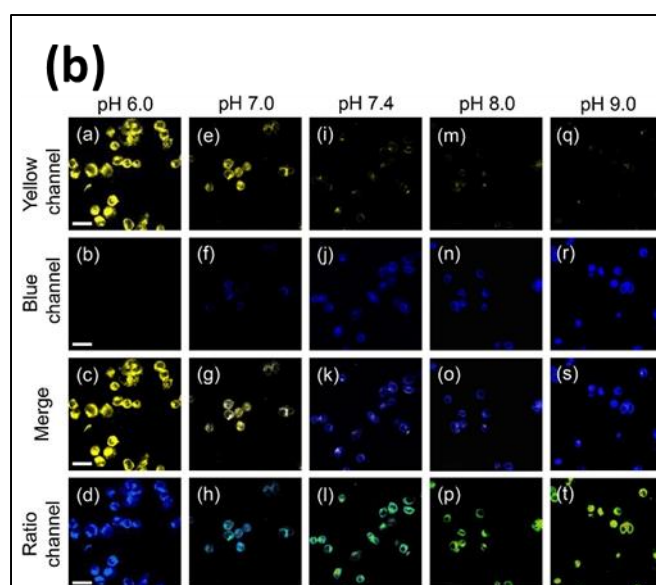
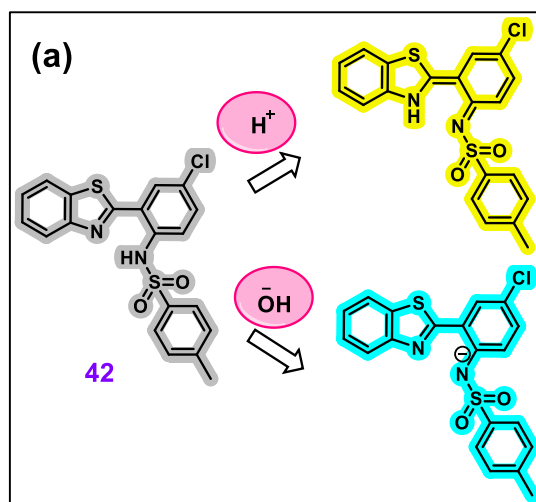


**Figure 36:** (a) Schematic representation of probe **42** for pH sensing. (b) Fluorescence cell imaging at different pHs using probe **42**. Reproduced with permission from [69].

Zeng *et al.*<sup>69</sup> developed electron withdrawing tosyl group derived amino-HBT based ratiometric fluorescent *turn-on* sensor **42** for pH in aqueous buffer: DMSO (99.5:0.5, (v/v)) environment. The ESIPT “*off*” state was initially observed due to the protecting tosyl group, which cleaved in acidic and basic media to exhibit yellow fluorescence and cyan-blue fluorescence, respectively. In acidic and basic media, large stokes shifts of 186 nm and 118 nm, fluorescence enhancement at 478 nm ( $\Phi = 0.58$ ) and 546 nm ( $\Phi = 0.40$ ) was observed, respectively. As shown in figure 36(b), **42** was explored for biological applications, which confirmed its capabilities to monitor the pH changes and visualize the pH fluctuations in living cells under oxidative stress.

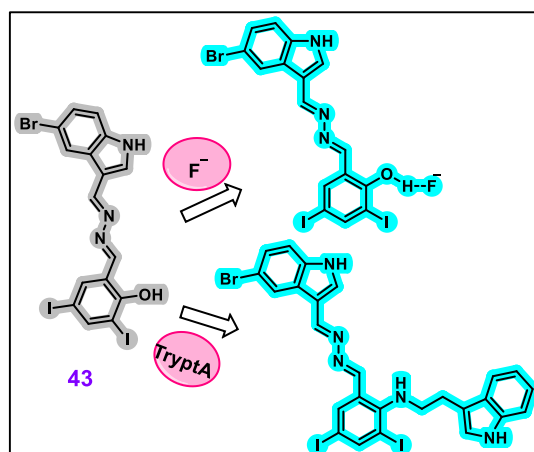


**Figure 37:** Chemical structure of probe **43** and mechanism for F<sup>-</sup> & TryptA sensing.

Ayyanar *et al.*<sup>70</sup> reported a colorimetric and *turn-on* emission probe **43** for anion (F<sup>-</sup>) and biogenic tryptamine (TryptA). TryptA addition triggered the ratiometric emission change with enhancement at 433 nm and the peak diminished at 555 nm with a hypsochromic shift of 28 nm in DMSO/H<sub>2</sub>O (9:1, v/v) solvent system. F<sup>-</sup> addition also induced similar spectral trends attributed to the deprotonation reaction along with orange (**43**) to yellow (**43-F<sup>-</sup>**) and light brown (**43-TryptA**) visual color changes. Uv-vis studies showed peak diminished at 372 nm whereas enhancement was recorded at 487 nm. HeLa cells treated with **43** exhibited fluorescence enhancement with fluoride. Furthermore, fluorescence enhancement in zebrafish embryos in the co-existence of TryptA confirms biological applications.

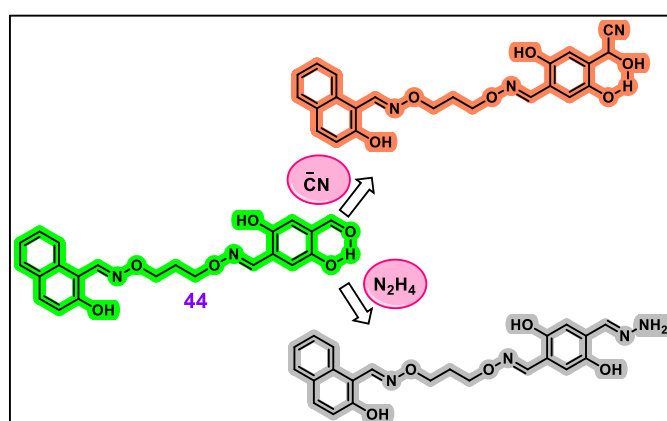


**Figure 38:** Schematic representation of probe **44** for CN<sup>-</sup> & hydrazine sensing.

Dong *et al.*<sup>71</sup> designed & synthesized multi-purpose probe **44** with unique ESIPT and RAHB (resonance-assisted hydrogen bonding) processes, for the detection of CN<sup>-</sup> and hydrazine in DMSO/H<sub>2</sub>O (v/v = 9/1, pH = 7.0). In absorbance, the broad absorbance band in the 450-500 nm region was attributed to the keto isomer (*ESIPT-on*). Both CN<sup>-</sup> & hydrazine showed fluorescence decrease at



477 nm and blue to orange-red (with  $\text{CN}^-$ ) naked eye detectable fluorescence change with 116 nm Stokes shift. **44** also showed an emission decrease with red-shift (20 nm) in different fractions of water which was attributed to aggregates formation. Further, **44** showed environmental applications by detecting  $\text{CN}^-$  in agricultural products, and test strips for direct detection of gaseous hydrazine.

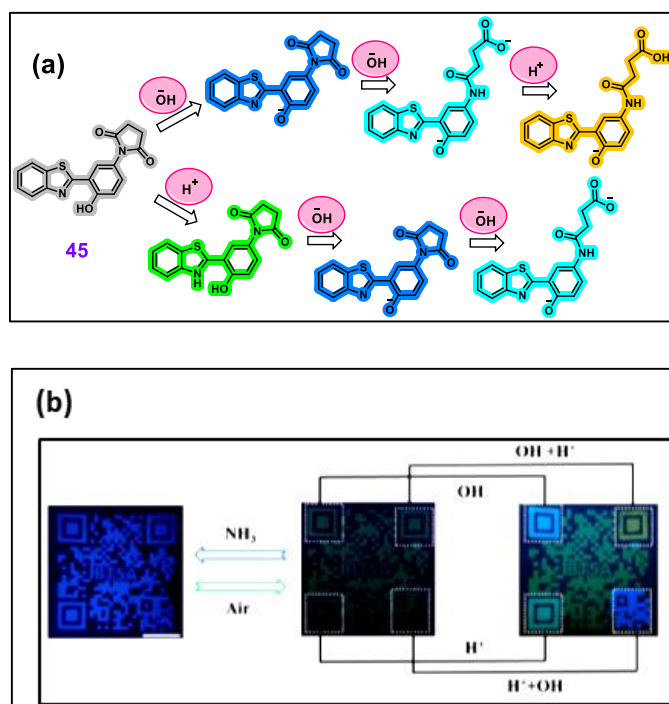


**Figure 39:** (a) Schematic representation of probe **45** for pH sensing. (b) Photographic images of reversible fluorescence change observed with  $\text{NH}_3/\text{air}$  and the different color changes observed in **45** with  $\text{H}^+$ ,  $\text{OH}^-$ ,  $\text{OH}^- + \text{H}^+$  and  $\text{H}^+ + \text{OH}^-$ . Reproduced with permission from [72].

Utilizing combined effect of AIE & ESIPT mechanisms, Xu *et al.*<sup>72</sup> developed a new strategy using HBT based probe **45** for monitoring food freshness and anti-counterfeiting by incorporating multiple pH-sensitive units. In the presence of base (NaOH), aggregation was disturbed due to deprotonation and **45** showed blue-shifted emission ( $\lambda_{\text{ex.}} = 365 \text{ nm}$ ) from 513nm to 458nm (AIE emission to enol emission). On further pH increment, bathochromic shifted emission due to the ring opening of the succinimide unit from 458 nm to 500 nm was recorded. Further, with the addition of  $\text{H}^+$ , protonation occurred to benzothiazole N and O and a spectral shift was recorded. The fluorescence color changes were detectable with the naked eyes and could be monitored with a smartphone. In the ammonia environment, reversible switching of the green and blue fluorescence was observed due to ESIPT *off*. The color changes could be helpful in developing detection methods for security purposes as shown in figure 39b. Furthermore, application of **45** were also explored in visual estimation pork and shrimp samples freshness.

## ESIPT based probes for Neutral molecules

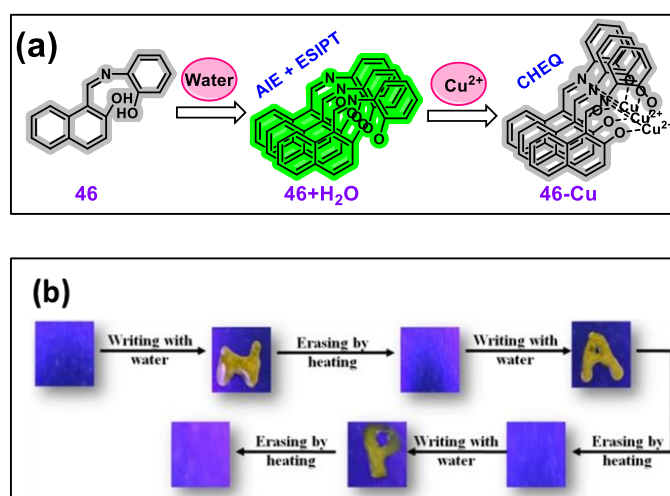


**Figure 40:** (a) Schematic representation of probe **46** for Cu<sup>2+</sup>. (b) Test paper-based inkless writing using fluorescence change. Reproduced from [73].

Schiff base containing imine group (-C=N-) with ortho -OH group to attain H-donor-acceptor properties can exhibit the ESIPT process. Utilizing similar structural modifications, Banerjee *et al.*<sup>73</sup> synthesized *turn-on* probe **46** for water with synergic photo-physical properties of AIE and ESIPT mechanism, this aggregated state was further employed for the *turn-off* sensor for Cu<sup>2+</sup>. With water, both AIE and ESIPT mechanisms in **46** exhibit enhancement in fluorescence ( $\lambda_{\text{ex.}} = 360 \text{ nm}$ ,  $\lambda_{\text{em.}} = 435\text{-}516 \text{ nm}$ ). The LOD of 0.033% (v/v, THF), 0.032% (v/v, acetone), 0.034% (v/v, DMSO), and 0.033% (v/v, MeOH) showed good sensitivity of **46** towards the water. Notably, **46** showed multiple applications such as trace level moisture detection in food samples, inkless writing for anti-counterfeiting activities (as shown in figure 40b) and on-site monitoring smartphone for moisture detection. In addition, **46** also displayed chelation-caused quenching with Cu<sup>2+</sup> in MeOH/H<sub>2</sub>O with LOD of 57.2 ppb and 1:1 binding stoichiometry.

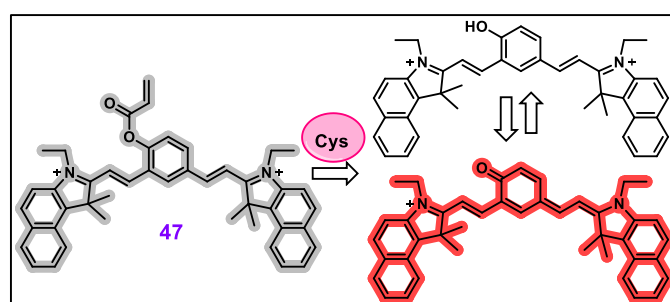


**Figure 41:** Chemical structure of probe **47** and mechanism for Cys sensing.

Chen and co-workers<sup>74</sup> reported NIR absorbing probe **47** for Cys with *turn-on* fluorescence at 726 nm ( $\lambda_{\text{ex.}} = 648$  nm) with high selectivity in HEPES: DMSO (99:1, v/v, pH 7.4). **47** consists of a cyanine dye-based NIR absorbing unit and fluorophore with acrylate group (Cys responsive unit) with a response time of 10 minutes for reaction completion. The absorbance band enhancement in 400-700 nm range and LOD of 0.15  $\mu\text{M}$  was recorded with Cys. Moreover, biological applications of **47** were confirmed by imaging endogenous Cys in different biological samples such as zebrafish, HT-22 cells, mice tissues and *in-vivo* studies in mice models.

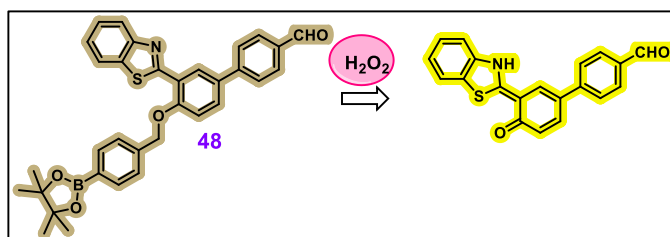


**Figure 42:** Chemical structure of probe **48** and mechanism for  $\text{H}_2\text{O}_2$  sensing.

Using  $\text{H}_2\text{O}_2$ -induced boronic ester oxidation and 1,6-elimination reaction, Jiang *et al.*<sup>75</sup> synthesized **48** based  $\text{H}_2\text{O}_2$  probe with ICT and ESIPT mechanisms with excellent selectivity and LOD of  $1.0 \times 10^{-6}$  M in PBS:ACN (3:1, v/v, pH 7.4). The  $\text{H}_2\text{O}_2$  mediated boronic ester oxidation followed by 1,6-elimination reaction cleaved the blocking group to give free-hydroxyl group ESIPT *on* state and thereby increase emission at 545 nm ( $\lambda_{\text{ex.}} = 350$  nm, stokes shift  $\sim 195$  nm). The *turn-on* response with  $\text{H}_2\text{O}_2$  was also observed in HeLa cells incubated with **48** under fluorescence cell imaging.

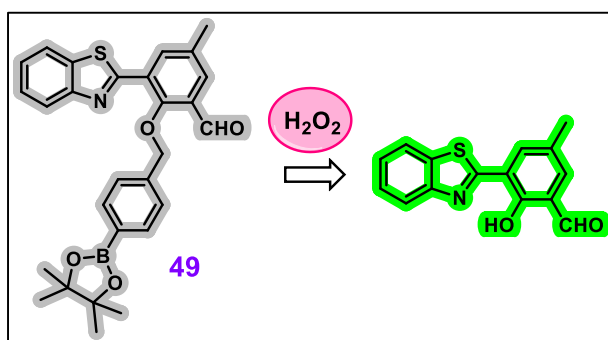


**Figure 43:** Chemical structure of probe **49** and mechanism for  $\text{H}_2\text{O}_2$  sensing.

Zhou *et al.*<sup>76</sup> developed pinacol phenyl borate ester-derived  $\text{H}_2\text{O}_2$  sensor **49** with HBT as fluorophore in ESIPT-*off* state. In absorbance,  $\text{H}_2\text{O}_2$  induced a rise in the Uv-vis intensity at 430 nm and showed fluorescence increment at 542 nm ( $\lambda_{\text{ex.}} = 380$  nm) in PBS:ACN (5:1, v/v, pH 7.4). The  $\text{H}_2\text{O}_2$  triggered conversion of boronic ester to phenol group and thereby ESIPT “on” state was responsible for *turn-on* emission.

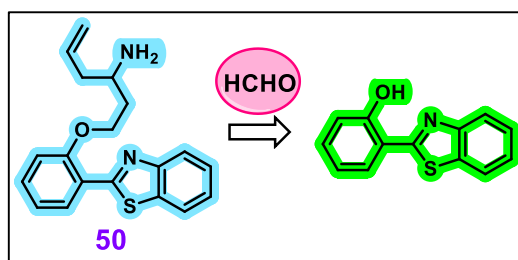


**Figure 44:** Chemical structure of probe **50** and mechanism for HCHO sensing.

For turn-on formaldehyde (FA) sensing, Chen *et al.*<sup>77</sup> constructed a 2-HBT based probe **50**. In EtOH/PBS (1 : 50, v/v, pH = 7.4) solvent, the initial emission at 380 nm ( $\lambda_{\text{ex}} = 340$  nm) exhibited a bathochromic shift to 520 nm in FA environment. The FA-triggered 2-aza-Cope rearrangement &  $\beta$ -elimination to detach HBT fluorophore from probe **50** and thereby ESIPT *on* state were responsible for spectral changes. Also, good biocompatibility, LOD of 66 nM, and detection of exogenous & endogenous FA in live cells support the biological application of **50**.

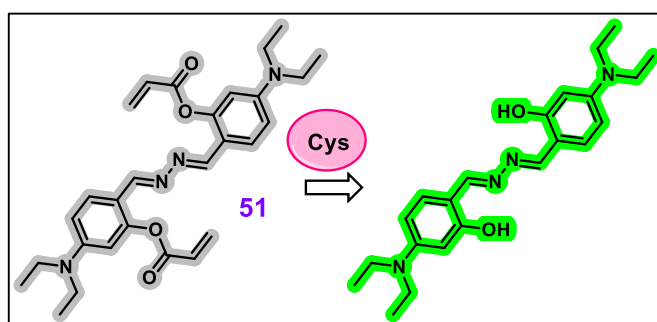


**Figure 45:** Chemical structure of probe **51** and mechanism for Cys sensing.

By exploiting the nucleophilic nature of  $\text{-SH}$  group, Ding *et al.*<sup>78</sup> synthesized probe **51** which exhibits enhancement in fluorescence in the Cys environment. The acrylate group acts as a reactive unit for Cys and ESIPT blocking unit. The chemical reaction between Cys & acrylate group produced a free fluorophore in ESIPT “on” state at 525 nm ( $\lambda_{\text{ex}} = 445$  nm) in PBS:EtOH (7:3, v/v, pH 7.4). With high selectivity, probe **51** showed a LOD of 36.4 nM and its utility in visualizing Cys in live cells and zebrafish confirmed the biological applications.

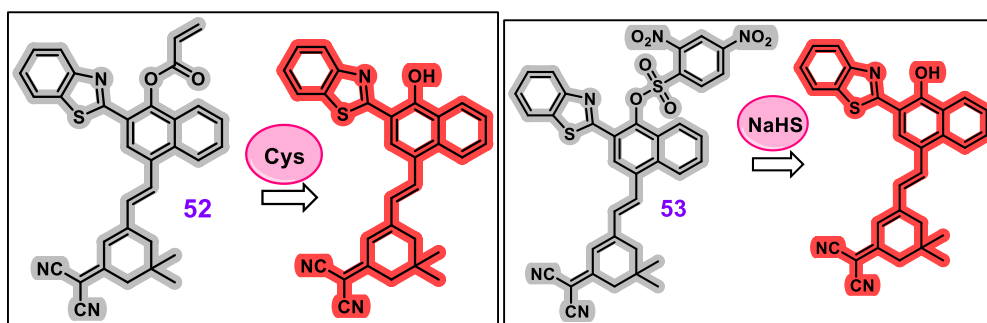


**Figure 46:** Schematic representation of probe **52** & **53** for Cys & H<sub>2</sub>S sensing.

Li *et al.*<sup>79</sup> developed NIR absorbing dicyanoisophosphorone fluorophore based probe **52** for Cys and **53** for H<sub>2</sub>S (NaHS). For **52** and **53**, acrylate unit and 2, 4-dinitrobenzene sulfonyl moiety act as the reactive unit and ESIPT blocking units, respectively. **52** showed good selectivity and sensitivity (LOD = 0.28 μM) for Cys over bio-thiols and can visualize endogenous Cys in tumor tissues. In case of **53**, good sensitivity was observed with emission increment at 766 nm which was attributed to 2, 4-dinitrobenzene sulfonyl unit detachment from fluorophore by H<sub>2</sub>S.

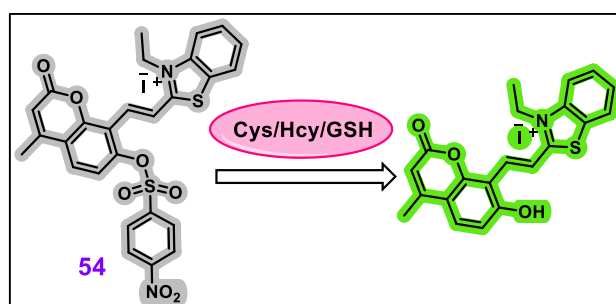


**Figure 47:** Schematic representation of probe **54** for Cys/GSH/Hcy sensing.

Bi *et al.*<sup>80</sup> reported Hcy/Cys/ GSH sensor **54**, which consists of a coumarin skeleton derived with EWG (4-nitrobenzene sulfonyl) blocking the -OH group and ESIPT off state. In emission, initial weak fluorescence was observed whereas fluorescence increase with bio-thiols was recorded at 500 nm ( $\lambda_{ex}=430\text{nm}$ ) in DMF:H<sub>2</sub>O (1:9, v/ v). In terms of mechanism, Hcy/Cys/ GSH cleaved the S-O bond thereby releasing the EW group with ESIPT “on” state. **54** showed good response time and biocompatibility supported by the *in-vitro* and *in-vivo* bio-thiol visualization in HeLa cells.

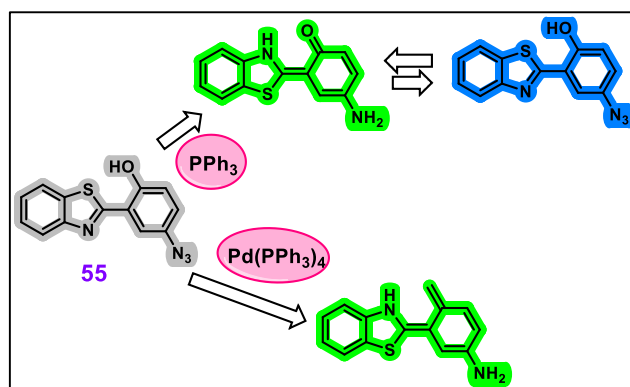


**Figure 48:** Schematic representation of probe **55** for PPh<sub>3</sub> and Pd(PPh<sub>3</sub>)<sub>4</sub> sensing.

Using the Staudinger reaction, Xu *et al.*<sup>81</sup> designed a 2-HBT-derived probe **55** with a free azido group for PPh<sub>3</sub> and Pd(PPh<sub>3</sub>)<sub>4</sub> detection in DMSO-HEPES (v/v, 1/1, pH 7.4). In Pd(PPh<sub>3</sub>)<sub>4</sub> environment, a rise in emission was observed at 526 nm in a semi-aqueous environment. Whereas, dual emission peak increase was observed at 443 nm and 526 nm, which showed the existence of keto-enol tautomeric forms. These changes were attributed to azide to amine conversion and consequent ESIPT “on” state. Further, PPh<sub>3</sub> visualization in live cells confirmed the biological applications and Pd(PPh<sub>3</sub>)<sub>4</sub> residues detection in organic reactions confirmed the utility of **55** to confirm the purity of organic products.

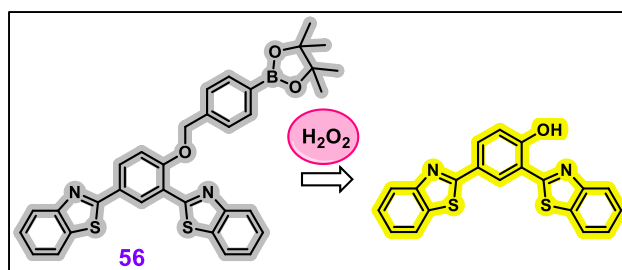


**Figure 49:** Chemical structure of probe **56** and mechanism for H<sub>2</sub>O<sub>2</sub> sensing.

Chen *et al.*<sup>82</sup> synthesized ESIPT and AIE mechanism-based H<sub>2</sub>O<sub>2</sub> probe **56** derived with benzothiazole fluorophores. **56** exhibited ESIPT-dependent AIE process and in the H<sub>2</sub>O<sub>2</sub> environment, **56** showed emission enhancement with red-shift from 405 nm (enol) to 550 nm (keto) with excellent selectivity and sensitivity with 0.22  $\mu$ M in THF:PBS (1:20, v/v, pH 7.4). The enhancement was attributed to H<sub>2</sub>O<sub>2</sub>-triggered boronic ester removal via phenylboronic oxidation followed by 1,6-elimination and resulting in free –OH exhibiting ESIPT “on” mechanism. Further, emission enhancement was also observed in MCF-7 cells due to endogenous H<sub>2</sub>O<sub>2</sub> monitoring under confocal microscopy.

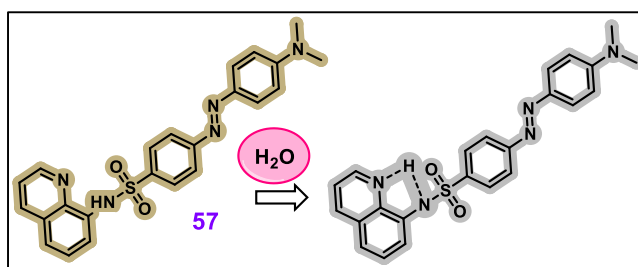


**Figure 50:** Chemical structure of probe **57** and mechanism for H<sub>2</sub>O sensing.

Kaushik *et al.*<sup>83</sup> have synthesized an 8-aminoquinoline fluorophore-based *turn-off* moisture sensor **57**. With excitation at 350 nm, high fluorescence “on” state was observed only in DMSO and THF solvents at 550 nm ( $\Phi=0.52\%$ ) and 530 nm ( $\Phi<0.1\%$ ), respectively. The LOD for moisture was reported as 0.0032(w/w%,DMSO) and 0.0014(w/w%,THF) confirming the excellent sensitivity of **57**. The ESIPT inhibition was confirmed by lifetime studies in DMSO.

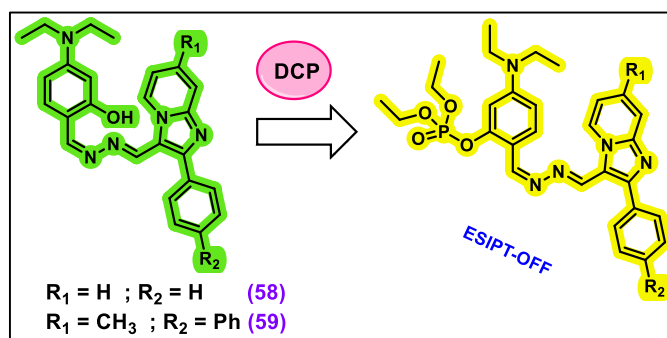


**Figure 51:** Chemical structure of probes **58** & **59** and mechanism for DCP sensing.

Sharma *et al.*<sup>84</sup> developed fused Imidazo[1,2-a]pyridine-based probes **58** and **59** for colourimetric and fluorescent detection of the nerve agents stimulants sarin (DCP) and tabun (DCNP) with quick response time in acetonitrile solvent. Initially, due to the free –OH group, probe **58** showed ESIPT “on” process and fluorescence maximum was recorded at 493 nm ( $\lambda_{ex.} = 414$  nm). The addition of DCP and DCNP showed a red shift in fluorescence maximum to 553 and 554, respectively. The LODs for DCP and DCNP using probe **58** were calculated as 4.3  $\mu$ M and 3.6  $\mu$ M, respectively. In the case of probe **59**, the initial fluorescence maximum at 503 nm showed a red-shift to 565 nm when DCP was added. Probe **59**, was also found to be selective with LOD of 0.6  $\mu$ M for DCP and showed no change with DCNP. Both probes **58** and **59**, showed colorimetric change under the UV lamp which was utilized for the naked-eye detection of DCP in vapour form using paper strips.

## Conclusion & Perspective

In conclusion, 59 examples of ESIPT-based probes were discussed based on the cations, anions and neutral species. These probes have been designed mainly by using benzothiazole unit, Coumarin unit,

flavonoid unit, pyrene unit, tetraphenylethene units etc. Compared to others, 2-HBT is mostly used as ESIPT active unit; hence, other fluorophores, such as Coumarin, tetraphenylethene, pyrene etc., must be considered for developing the probes. Mostly, two strategies are utilized for on-off switching of ESIPT signal: a) by blocking the –NH or –OH groups with EWG to form ESIPT off, and thereby removing/detaching EWG by specific analytes to get ESIPT on state, and b) imine group with an ortho-hydroxyl group in Schiff base which can act as keto-enol tautomerism. The imine group-based strategy is better than the time-consuming analytes-assisted removal of EWG from the fluorophore. Only limited examples that exhibit dual fluorescence mechanisms, i.e. AIE, CHEF, and PET-assisted ESIPT for detection are reported. Therefore, more probes can be developed with multiple fluorescence mechanisms to induce multi-channel emission and enhance the selectivity & sensitivity of analytes. The majority of the ESIPT probes are used for advanced biological applications by directly monitoring their fluorescence change. These probes exhibit a spectral change in the 350-550 nm region with blue or green fluorescent colors which is non-favorable for *in-vivo* and *in-vitro* fluorescence imaging studies. Therefore, significant attention is required to develop NIR (600-800 nm) absorbing ESIPT probes to circumvent concerns such as scattering/reabsorption of light, interference of chromophores present in the biological model, etc.

Overall, ESIPT-based probes have shown critical applications in multiple fields but still there is scope for improving their structural design and photo-physical properties. Further, ESIPT probes are expected to play an important role in developing newer strategies and advancements in medical imaging and early diagnosis of life-threatening diseases. These strategies may include structural modification of probes to achieve synergistic effects of ESIPT-AIE, ESIPT-FRET, ESIPT-ICT, ESIPT based two-photo fluorescent probes etc. which can provide excellent photo-stability, deep tissue penetration, low-auto fluorescence and high sensitivity for detection of analytes.



**Table 1: List of abbreviations**

ESIPT	Excited State Intramolecular Proton Transfer
μM	Micro molar
nM	Nano molar
UV-vis	Ultraviolet-Visible
ICT	Intramolecular Charge Transfer
PET	Photo-induced Electron Transfer
CHEF	Chelation Enhanced Fluorescence
AIE	Aggregation Induced Emission
2-HBI	2-(2'-hydroxyphenyl) benzimidazole
2-HBO	2-(2'-hydroxyphenyl) benzoxazole
2-HBT	2-(2'-hydroxyphenyl)benzothiazole
H-bond	Hydrogen bond
PPi	Pyrophosphate
LOD	Limit of Detection
λ <sub>ex</sub>	Excitation wavelength
DFT	Density Functional Theory
DMF	N,N-dimethyl formamide
TLC	Thin Layer Chromatography
CuAAC	Copper-catalyzed azide-alkyne cycloaddition
ACN	Acetonitrile
DCM	Dichloromethane
THF	Tetrahydrofuran
HEPES	(N-2-hydroxyethylpiperazine-N-2-ethane sulfonic acid)
DMSO	Dimethyl sulfoxide
EWG	Electron-withdrawing group

D- $\pi$ -A	Donor-pi-acceptor
Cys	Cysteine
PPi	Pyrophosphate
PMA	Phorbol-12-myristate-13-acetate
LPS	Lipopolysaccharide
IFN- $\gamma$	Interferon- $\gamma$
MeOH	Methanol
TryptA	Tryptamine
ppb	Parts per billion
FA	Formaldehyde
Hcy	Homo-cysteine
GSH	Glutathione
NIR	Near Infra-red

### Author contributions CRediT:

Nidhi Nehra: Writing – original draft; Rahul Kaushik: Writing – original draft, review & editing

### Acknowledgement

RK is grateful to The Director, CSIR-NIO, India for his support and encouragement. RK would like to acknowledge funding from project OLP 2006. NN would like to acknowledge The Director, IACS and the Director, IIT Bombay for the Institute Post-Doctoral fellowship.

### Conflicts of Interest

There are no conflicts of interest to declare.

### References

1. Krämer, J.; Kang, R.; Grimm, L. M.; De Cola, L.; Picchetti, P.; Biedermann, F., Molecular Probes, Chemosensors, and Nanosensors for Optical Detection of Biorelevant Molecules and Ions in Aqueous Media and Biofluids. *Chemical Reviews* **2022**, *122* (3), 3459-3636.
2. Singh, H.; Tiwari, K.; Tiwari, R.; Pramanik, S. K.; Das, A., Small Molecule as Fluorescent Probes for Monitoring Intracellular Enzymatic Transformations. *Chemical Reviews* **2019**, *119* (22), 11718-11760.

3. Fang, H.; Chen, Y.; Jiang, Z.; He, W.; Guo, Z., Fluorescent Probes for Biological Species and Microenvironments: from Rational Design to Bioimaging Applications. *Accounts of Chemical Research* **2023**, *56* (3), 258-269.
4. Kaushik, R.; Nehra, N.; Novakova, V.; Zimcik, P., Near-Infrared Probes for Biothiols (Cysteine, Homocysteine, and Glutathione): A Comprehensive Review. *ACS Omega* **2023**, *8* (1), 98-126.
5. Ghosh, A.; Jose, D. A.; Kaushik, R., Anthraquinones as versatile colorimetric reagent for anions. *Sensors and Actuators B: Chemical* **2016**, *229*, 545-560.
6. Jose, D. A.; Sakla, R.; Sharma, N.; Gadiyaram, S.; Kaushik, R.; Ghosh, A., Sensing and Bioimaging of the Gaseous Signaling Molecule Hydrogen Sulfide by Near-Infrared Fluorescent Probes. *ACS Sensors* **2020**, *5* (11), 3365-3391.
7. Kaushik, R.; Ghosh, A.; Amilan Jose, D., Recent progress in hydrogen sulphide (H<sub>2</sub>S) sensors by metal displacement approach. *Coordination Chemistry Reviews* **2017**, *347*, 141-157.
8. Kaushik, R.; Kumar, P.; Ghosh, A.; Gupta, N.; Kaur, D.; Arora, S.; Jose, D. A., Alizarin red S–zinc(ii) fluorescent ensemble for selective detection of hydrogen sulphide and assay with an H<sub>2</sub>S donor. *RSC Advances* **2015**, *5* (97), 79309-79316.
9. Kaushik, R.; Ghosh, A.; Jose, D. A., Simple terpyridine based Cu(II)/Zn(II) complexes for the selective fluorescent detection of H<sub>2</sub>S in aqueous medium. *Journal of Luminescence* **2016**, *171*, 112-117.
10. Kaushik, R.; Ghosh, A.; Singh, A.; Gupta, P.; Mittal, A.; Jose, D. A., Selective Detection of Cyanide in Water and Biological Samples by an Off-the-Shelf Compound. *ACS Sensors* **2016**, *1* (10), 1265-1271.
11. Ghosh, A.; Das, P.; Kaushik, R.; Damodaran, K. K.; Jose, D. A., Anion responsive and morphology tunable tripodal gelators. *RSC Advances* **2016**, *6* (86), 83303-83311.
12. Kaushik, R.; Singh, A.; Ghosh, A.; Jose, D. A., Selective Colorimetric Sensor for the Detection of Hg<sup>2+</sup> and H<sub>2</sub>S in Aqueous Medium and Waste Water Samples. *ChemistrySelect* **2016**, *1* (8), 1533-1540.
13. Iftikhar, R.; Parveen, I.; Ayesha; Mazhar, A.; Iqbal, M. S.; Kamal, G. M.; Hafeez, F.; Pang, A. L.; Ahmadipour, M., Small organic molecules as fluorescent sensors for the detection of highly toxic heavy metal cations in portable water. *Journal of Environmental Chemical Engineering* **2023**, *11* (1), 109030.
14. Liu, Y.; Jiao, C.; Lu, W.; Zhang, P.; Wang, Y., Research progress in the development of organic small molecule fluorescent probes for detecting H<sub>2</sub>O<sub>2</sub>. *RSC Advances* **2019**, *9* (31), 18027-18041.
15. Manna, S. K.; Achar, T. K.; Mondal, S., Recent advances in selective formaldehyde detection in biological and environmental samples by fluorometric and colorimetric chemodosimeters. *Analytical Methods* **2021**, *13* (9), 1084-1105.

16. Kumar, P.; Kaushik, R.; Ghosh, A.; Jose, D. A., Detection of Moisture by Fluorescent OFF-ON Sensor in Organic Solvents and Raw Food Products. *Analytical Chemistry* **2016**, *88* (23), 11314-11318.
17. Kumar, P.; Ghosh, A.; Jose, D. A., Chemical Sensors for Water Detection in Organic Solvents and their Applications. *ChemistrySelect* **2021**, *6* (4), 820-842.
18. Nehra, N.; Ghule, V. D.; Tittal, R. K., Simpler fluorescent probe for homocysteine selective detection. *Journal of Molecular Structure* **2022**, *1250*, 131755.
19. Nehra, N.; Kaushik, R.; Vikas D, G.; Tittal, R. K., Simpler molecular structure as selective & sensitive ESIPT-based fluorescent probe for cysteine and Homocysteine detection with DFT studies. *Journal of Molecular Structure* **2020**, *1207*, 127839.
20. Carter, K. P.; Young, A. M.; Palmer, A. E., Fluorescent Sensors for Measuring Metal Ions in Living Systems. *Chemical Reviews* **2014**, *114* (8), 4564-4601.
21. Naithani, S.; Goswami, T.; Thetiot, F.; Kumar, S., Imidazo[4,5-f][1,10]phenanthroline based luminescent probes for anion recognition: Recent achievements and challenges. *Coordination Chemistry Reviews* **2023**, *475*, 214894.
22. Tay, H. M.; Beer, P., Optical sensing of anions by macrocyclic and interlocked hosts. *Organic & Biomolecular Chemistry* **2021**, *19* (21), 4652-4677.
23. Park, S.-H.; Kwon, N.; Lee, J.-H.; Yoon, J.; Shin, I., Synthetic ratiometric fluorescent probes for detection of ions. *Chemical Society Reviews* **2020**, *49* (1), 143-179.
24. Dongare, P. R.; Gore, A. H., Recent Advances in Colorimetric and Fluorescent Chemosensors for Ionic Species: Design, Principle and Optical Signalling Mechanism. *ChemistrySelect* **2021**, *6* (23), 5657-5669.
25. Goshisht, M. K.; Tripathi, N., Fluorescence-based sensors as an emerging tool for anion detection: mechanism, sensory materials and applications. *Journal of Materials Chemistry C* **2021**, *9* (31), 9820-9850.
26. Lu, X.-L.; He, W., Research Advances in Excited State Intramolecular Proton Transfer Fluorescent Probes Based on Combined Fluorescence Mechanism. *Chinese Journal of Analytical Chemistry* **2021**, *49* (2), 184-196.
27. Sedgwick, A. C.; Wu, L.; Han, H.-H.; Bull, S. D.; He, X.-P.; James, T. D.; Sessler, J. L.; Tang, B. Z.; Tian, H.; Yoon, J., Excited-state intramolecular proton-transfer (ESIPT) based fluorescence sensors and imaging agents. *Chemical Society Reviews* **2018**, *47* (23), 8842-8880.
28. Gu, H.; Wang, W.; Wu, W.; Wang, M.; Liu, Y.; Jiao, Y.; Wang, F.; Wang, F.; Chen, X., Excited-state intramolecular proton transfer (ESIPT)-based fluorescent probes for biomarker detection: design, mechanism, and application. *Chemical Communications* **2023**, *59* (15), 2056-2071.
29. Li, Y.; Dahal, D.; Abeywickrama, C. S.; Pang, Y., Progress in Tuning Emission of the Excited-State Intramolecular Proton Transfer (ESIPT)-Based Fluorescent Probes. *ACS Omega* **2021**, *6* (10), 6547-6553.

30. Fery-Forgues, S.; Vanucci-Bacqué, C., Recent Trends in the Design, Synthesis, Spectroscopic Behavior, and Applications of Benzazole-Based Molecules with Solid-State Luminescence Enhancement Properties. *Topics in Current Chemistry* **2021**, 379 (5), 32.
31. Gayathri, P.; Pannipara, M.; Al-Sehemi, A. G.; Anthony, S. P., Recent advances in excited state intramolecular proton transfer mechanism-based solid state fluorescent materials and stimuli-responsive fluorescence switching. *CrystEngComm* **2021**, 23 (21), 3771-3789.
32. Sharma, S.; Ghosh, K. S., Recent advances (2017–20) in the detection of copper ion by using fluorescence sensors working through transfer of photo-induced electron (PET), excited-state intramolecular proton (ESIPT) and Förster resonance energy (FRET). *Spectrochimica Acta Part A: Molecular and Biomolecular Spectroscopy* **2021**, 254, 119610.
33. Wang, T.; Pang, Q.; Tong, Z.; Wang, M.; Xiao, N., Selective sensing of PPI by fluorogenic Al(III)-probe complex in aqueous medium. *Spectrochimica Acta Part A: Molecular and Biomolecular Spectroscopy* **2021**, 250, 119249.
34. Bhosle, A. A.; Hiremath, S. D.; Bhasikuttan, A. C.; Banerjee, M.; Chatterjee, A., Solvent-free mechanochemical synthesis of a novel benzothiazole-azine based ESIPT-coupled orange AIEgen for the selective recognition of Cu<sup>2+</sup> ions in solution and solid phase. *Journal of Photochemistry and Photobiology A: Chemistry* **2021**, 413, 113265.
35. Nehra, N.; Tittal, R. K.; Ghule, V. D., 1,2,3-Triazoles of 8-Hydroxyquinoline and HBT: Synthesis and Studies (DNA Binding, Antimicrobial, Molecular Docking, ADME, and DFT). *ACS Omega* **2021**, 6 (41), 27089-27100.
36. Mondal, S.; Dey, S., Strategy to Design a Flexible and Macromolecular Sensor to Bind Cd<sup>2+</sup> Ions: A Complete Photophysical Analysis and Bio-Imaging Study. *ACS Omega* **2021**, 6 (42), 27936-27945.
37. Gong, F.; Zeng, D.; Zhu, H.; Qian, Y.; He, L.; Xia, J.; Cao, Z., A solvent-assisted ESIPT fluorescent dye for F<sup>-</sup>/Ag<sup>+</sup> sensing and high-resolution imaging of the cilia in live cells. *Analytical and Bioanalytical Chemistry* **2021**, 413 (25), 6343-6353.
38. Gayathri, P.; Kanagajothi, K.; Nag, P.; Anand, N.; Reddy, V. S.; Moon, D.; Anthony, S. P.; Madhu, V., Symmetrical and unsymmetrical thiazole-based ESIPT derivatives: the highly selective fluorescence sensing of Cu<sup>2+</sup> and structure-controlled reversible mechanofluorochromism. *CrystEngComm* **2021**, 23 (38), 6769-6777.
39. Sun, H.; Jiang, Y.; Nie, J.; Wei, J.; Miao, B.; Zhao, Y.; Zhang, L.; Ni, Z., Multifunctional AIE-ESIPT dual mechanism tetraphenylethene-based Schiff base for inkless rewritable paper and a colorimetric/fluorescent dual-channel Zn<sup>2+</sup> sensor. *Materials Chemistry Frontiers* **2021**, 5 (1), 347-354.
40. Pariat, T.; Vérité, P. M.; Jacquemin, D.; Massue, J.; Ulrich, G., 2,2-Dipicolylamino substituted 2-(2'-hydroxybenzofuranyl) benzoxazole (HBBO) derivative: Towards ratiometric sensing of divalent zinc cations. *Dyes and Pigments* **2021**, 190, 109338.
41. Wang, L.; Chen, H.; Zhang, N.; Liu, X.; Zheng, K., Reaction-based two novel fluorescent probes for Hg<sup>2+</sup> detection using benzothiazole derivatives via ESIPT mechanism in aqueous solution and serum. *Tetrahedron Letters* **2021**, 64, 152735.

42. Zheng, H.-W.; Kang, Y.; Wu, M.; Liang, Q.-F.; Zheng, J.-Q.; Zheng, X.-J.; Jin, L.-P., ESIPT-AIE active Schiff base based on 2-(2'-hydroxyphenyl)benzo-thiazole applied as multi-functional fluorescent chemosensors. *Dalton Transactions* **2021**, 50 (11), 3916-3922.
43. Zhu, M.; Huang, S.; Chen, M.; Li, Y.; Zhong, M., A novel Schiff's base conjugate with multicolor changes in multiple states and its multipurpose applications for selective detection of Cu<sup>2+</sup> in aggregated state and on silica gel strip. *Optical Materials* **2022**, 127, 112288.
44. Al Anshori, J.; Ismalah, D.; Abror, A. F.; Zainuddin, A.; Wiani Hidayat, I.; Yusuf, M.; Maharani, R.; Tatang Hidayat, A., A new highly selective "off-on" typical chemosensor of Al<sup>3+</sup>, 1-((Z)-((E)-(3,5-dichloro-2-hydroxybenzylidene)hydrazono)methyl) naphthalene-2-ol, an experimental and in silico study. *RSC Advances* **2022**, 12 (5), 2972-2979.
45. Arabahmadi, R., Hydrazone-based Schiff base dual chemosensor for recognition of Cu<sup>2+</sup> and F<sup>-</sup> by 1:2 demultiplexer, half adder, half subtractor, molecular keypad lock and logically reversible transfer gate logic circuits and its application as test kit. *Journal of Photochemistry and Photobiology A: Chemistry* **2022**, 427, 113797.
46. Piyanuch, P.; Wangngae, S.; Kamkaew, A.; Wattanathana, W.; Wannapaiboon, S.; Impeng, S.; Maneprakorn, W.; Promarak, V.; Chansaenpak, K., Ultrasensitive fluorogenic chemosensor based on ESIPT phenomenon for selective determination of Cu<sup>2+</sup> ion in aqueous system and its application in environmental samples and biological imaging. *Dyes and Pigments* **2022**, 205, 110532.
47. Bag, R.; Sikdar, Y.; Sahu, S.; Das Mukhopadhyay, C.; Drew, M. G. B.; Goswami, S., Benzimidazole based ESIPT active chemosensors enable nano-molar detection of Cu<sup>2+</sup> in 90% aqueous solution, MCF-7 cells, and plants. *Journal of Photochemistry and Photobiology A: Chemistry* **2022**, 431, 114006.
48. Wang, D.; Li, S.-J.; Cao, W.; Wang, Z.; Ma, Y., ESIPT-Active 8-Hydroxyquinoline-Based Fluorescence Sensor for Zn(II) Detection and Aggregation-Induced Emission of the Zn(II) Complex. *ACS Omega* **2022**, 7 (21), 18017-18026.
49. Santhiya, K.; Mathivanan, M.; Tharmalingam, B.; Anitha, O.; Ghorai, S.; Natarajan, R.; Murugesapandian, B., A new 7-(diethylamino)coumarin and 4-(diethylamino)phenol appended unsymmetrical thiocarbohydrazone: Detection of moisture in organic solvent and sequential fluorimetric detection of Cu<sup>2+</sup> ions and cysteine. *Journal of Photochemistry and Photobiology A: Chemistry* **2022**, 432, 114105.
50. Gadiyaram, S.; Ghule, V. D.; Ghosh, A.; Jose, D. A., An ESIPT-based fluorescent probe for the detection of multiple analytes and a facile approach to discriminate between arsenate and pyrophosphate in water. *Sensors & Diagnostics* **2022**, 1 (6), 1224-1235.
51. Thomas, H.; Naimhwaka, J.; Endjala, P.; Uahengo, V., ESIPT-influenced C<sub>3</sub>-symmetry, disk-shaped fluorescence turn-on probe for Zn<sup>2+</sup> based on melamine-naphthyl moiety with high affinity towards Cu<sup>2+</sup> in CH<sub>3</sub>CN. *Results in Optics* **2022**, 6, 100215.
52. Mei, H.; Yang, C.; Yang, X.; Huang, Z.; Cheng, P.; Xu, K., A novel reversible oxazole-based NIR fluorescent probe for Cu<sup>2+</sup> and S<sup>2-</sup> ions detection. *Journal of Molecular Structure* **2022**, 1266, 133522.

53. Kaur, R.; Kour, R.; Marok, S. S.; Kaur, S.; Singh, P. AIE+ESIPT Active Hydroxybenzothiazole for Intracellular Detection of Cu<sup>2+</sup>: Anticancer and Anticounterfeiting Applications *Molecules* [Online], 2022.
54. Bai, C.; Zhang, J.; Ma, W.; Yao, J.; Meng, Q.; Xia, Z.; Chen, D.; He, S.; Zhang, L.; Qu, C.; Qiao, R.; Yang, Z.; Huang, W., A new intramolecular proton transfer (ESIPT)-based fluorescent probe for selective visualization of cyanide ion. *VIEW* **2022**, *n/a* (n/a), 20220068.
55. Zhu, T.; Hu, Y.; Chen, X.; Shao, H.; Chen, Z.; Zhang, H.; Liu, C., Novel chromene-derived fluorescent probe for detection of cyanides by imine-controlled ESIPT. *Dyes and Pigments* **2021**, *195*, 109693.
56. Sun, Y.; Tang, X.; Li, X.; Kong, X.; Tian, M.; Wang, Y.; Dong, B., PET-ESIPT-based fluorescent probes for revealing the fluctuation of peroxynitrite (ONOO<sup>-</sup>) in living cells, zebrafishes and brain tissues. *Sensors and Actuators B: Chemical* **2022**, *353*, 131121.
57. Yu, J.; Shu, W.; Kang, H.; Han, R.; Zhang, X.; Zhang, R.; Jing, J.; Zhang, X., An ESIPT-based fluorescent probe with large Stokes shift for peroxynitrite detection in HeLa cells and zebrafish. *Dyes and Pigments* **2022**, *204*, 110334.
58. Du, Y.; Wang, H.; Qin, L.; Zhao, M.; Pan, C., Rational development of an ESIPT-based fluorescent probe with large Stokes shift for imaging of hydrogen sulfide in live cells. *Bioorganic Chemistry* **2022**, *129*, 106158.
59. Du, Y.; Wang, H.; Zhang, T.; Wen, W.; Li, Z.; Bi, M.; Liu, J., An ESIPT-based fluorescent probe with fast-response for detection of hydrogen sulfide in mitochondria. *Spectrochimica Acta Part A: Molecular and Biomolecular Spectroscopy* **2022**, *265*, 120390.
60. Wu, L.; Tian, X.; Lee, D. J.; Yoon, J.; Lim, C. S.; Kim, H. M.; James, T. D., Two-photon ESIPT-based fluorescent probe using 4-hydroxyisoindoline-1,3-dione for the detection of peroxynitrite. *Chemical Communications* **2021**, *57* (84), 11084-11087.
61. Tian, Y.; Che, H.; Wang, J.; Wang, D.; Yang, L.; Wang, L.; Nie, Y.; Tian, X., Smartphone as a simple device for visual and on-site detection of fluoride in groundwater. *Journal of Hazardous Materials* **2021**, *411*, 125182.
62. Gu, B.; Wu, C.; Zhang, C.; He, S.; Tang, S.; Li, H.; Shen, Y., A morpholino hydrazone-based lysosome-targeting fluorescent probe with fast response and high sensitivity for imaging peroxynitrite in living cells. *Spectrochimica Acta Part A: Molecular and Biomolecular Spectroscopy* **2021**, *262*, 120100.
63. Qu, W.; Guo, T.; Yang, B.; Tian, R.; Qiu, S.; Chen, X.; Geng, Z.; Wang, Z., Tracking HOCl by an incredibly simple fluorescent probe with AIE plus ESIPT in vitro and in vivo. *Spectrochimica Acta Part A: Molecular and Biomolecular Spectroscopy* **2022**, *281*, 121649.
64. Kim, J. K.; Bong, S. Y.; Park, R.; Park, J.; Jang, D. O., An ESIPT-based fluorescent turn-on probe with isothiocyanate for detecting hydrogen sulfide in environmental and biological systems. *Spectrochimica Acta Part A: Molecular and Biomolecular Spectroscopy* **2022**, *278*, 121333.
65. Ren, H.; Huo, F.; Yin, C., An ESIPT-based colorimetric and fluorescent probe with large Stokes shift for the sensitive detection of hypochlorous acid and its bioimaging in cells. *New Journal of Chemistry* **2021**, *45* (10), 4724-4728.

66. Fang, S.; Wang, L.; Mei, Y.; Zheng, K., A ratiometric fluorescent probe for sensing hypochlorite in physiological saline, bovine serum albumin and fetal bovine/calf serum. *Spectrochimica Acta Part A: Molecular and Biomolecular Spectroscopy* **2022**, *269*, 120738.
67. Abeywickrama, C. S.; Pang, Y., Synthesis of a bis[2-(2'-hydroxyphenyl)benzoxazole]pyridinium derivative: the fluoride-induced large spectral shift for ratiometric response. *New Journal of Chemistry* **2021**, *45* (20), 9102-9108.
68. Kafuti, Y. S.; Zeng, S.; Qian, M.; Zhang, C.; Liu, X.; Wang, J.; Chen, Q., A novel NIR fluorescent probe with fast response and large stokes shift for the detection and imaging of hypochlorous acid in living cells. *Dyes and Pigments* **2022**, *199*, 110067.
69. Feng, B.; Zhu, Y.; Wu, J.; Huang, X.; Song, R.; Huang, L.; Feng, X.; Zeng, W., Monitoring intracellular pH fluctuation with an excited-state intramolecular proton transfer-based ratiometric fluorescent sensor. *Chinese Chemical Letters* **2021**, *32* (10), 3057-3060.
70. Karupiah, K.; Nelson, M.; Alam, M. M.; Selvaraj, M.; Sepperumal, M.; Ayyanar, S., A new 5-bromoindolehydrazone anchored diiodosalicylaldehyde derivative as efficient fluoro and chromophore for selective and sensitive detection of tryptamine and F<sup>-</sup> ions: Applications in live cell imaging. *Spectrochimica Acta Part A: Molecular and Biomolecular Spectroscopy* **2022**, *269*, 120777.
71. Chen, Z.-Z.; Deng, Y.-H.; Zhang, T.; Dong, W.-K., A novel bifunctional-group salamo-like multi-purpose dye probe based on ESIPT and RAHB effect: Distinction of cyanide and hydrazine through optical signal differential protocol. *Spectrochimica Acta Part A: Molecular and Biomolecular Spectroscopy* **2021**, *262*, 120084.
72. Zhang, Q.; Yang, L.; Han, Y.; Wang, Z.; Li, H.; Sun, S.; Xu, Y., A pH-sensitive ESIPT molecule with aggregation-induced emission and tunable solid-state fluorescence multicolor for anti-counterfeiting and food freshness detection. *Chemical Engineering Journal* **2022**, *428*, 130986.
73. Das, R.; Bej, S.; Hirani, H.; Banerjee, P., Trace-Level Humidity Sensing from Commercial Organic Solvents and Food Products by an AIE/ESIPT-Triggered Piezochromic Luminogen and ppb-Level "OFF-ON-OFF" Sensing of Cu<sup>2+</sup>: A Combined Experimental and Theoretical Outcome. *ACS Omega* **2021**, *6* (22), 14104-14121.
74. Zhang, X.; Zhang, L.; Wang, X.; Han, X.; Huang, Y.; Li, B.; Chen, L., Visualizing and evaluating mitochondrial cysteine via near-infrared fluorescence imaging in cells, tissues and in vivo under hypoxia/reperfusion stress. *Journal of Hazardous Materials* **2021**, *419*, 126476.
75. Tang, J.; Li, F.; Liu, C.; Shu, J.; Yue, J.; Xu, B.; Liu, X.; Zhang, K.; Jiang, W., Attractive benzothiazole-based fluorescence probe for the highly efficient detection of hydrogen peroxide. *Analytica Chimica Acta* **2022**, *1214*, 339939.
76. Zhang, H.-C.; Tian, D.-H.; Zheng, Y.-L.; Dai, F.; Zhou, B., Designing an ESIPT-based fluorescent probe for imaging of hydrogen peroxide during the ferroptosis process. *Spectrochimica Acta Part A: Molecular and Biomolecular Spectroscopy* **2021**, *248*, 119264.
77. Quan, T.; Liang, Z.; Pang, H.; Zeng, G.; Chen, T., A ratiometric ESIPT probe based on 2-aza-Cope rearrangement for rapid and selective detection of formaldehyde in living cells. *Analyst* **2022**, *147* (2), 252-261.



78. Guo, X.; Wan, C.; Li, J.; Xiao, Y.; Cao, Q.; Zhang, Q.; Zhang, P.; Ding, C., Hydrogen bond driven fluorescent lighting up for cysteine based on excited state intramolecular proton transfer process. *Dyes and Pigments* **2022**, *197*, 109880.
79. Qin, J.; Tian, H.; Kong, F.; Zhao, Q. q.; Zhang, C.; Gu, H.; Li, Y., A novel long excitation/emission wavelength fluorophore as platform utilized to construct NIR probes for bioimaging and biosensing. *Bioorganic Chemistry* **2022**, *127*, 105954.
80. Ding, G.; Wang, X.; Luo, D.; Meng, S.; Zhou, L.; Fan, Y.; Ling-hu, C.; Meng, J.; Si, W.; Chen, Q.; Bi, R., A simple ESIPT combines AIE character “turn on” fluorescent probe for Hcy/Cys/GSH detection and cell imaging based on coumarin unit. *Dyes and Pigments* **2022**, *208*, 110762.
81. Zhang, Y.; Li, H.; Sun, S.; Xu, Y., An ESIPT fluorescent probe based on Staudinger reaction for detection of triphenylphosphine and tetrakis(triphenyl-phosphine)palladium. *Sensors and Actuators B: Chemical* **2022**, *358*, 131506.
82. Zeng, G.; Liang, Z.; Jiang, X.; Quan, T.; Chen, T., An ESIPT-Dependent AIE Fluorophore Based on HBT Derivative: Substituent Positional Impact on Aggregated Luminescence and its Application for Hydrogen Peroxide Detection. *Chemistry – A European Journal* **2022**, *28* (5), e202103241.
83. Kaushik, R.; Sakla, R.; Kumar, N.; Ghosh, A.; Ghule, V. D.; Jose, D. A., Multianalytes Sensing Probe: Fluorescent Moisture Detection, Smartphone Assisted Colorimetric Phosgene recognition and Colorimetric Discrimination of Cu<sup>2+</sup> and Fe<sup>3+</sup> ions. *Sensors and Actuators B: Chemical* **2021**, *328*, 129026.
84. Thakur, A.; Sharma, A., Imidazo[1,2-a]pyridine based small organic fluorescent molecules for selective detection of nerve agents simulants. *Spectrochimica Acta Part A: Molecular and Biomolecular Spectroscopy* **2022**, *282*, 121633.